α-Phenylalanyl tRNA synthetase competes with Notch signaling through its N-terminal domain

Manh Tin Ho[1], Jiongming Lu[2], Paula Vazquez-Pianzola[1], Beat Suter[1]

Affiliations:

[1]Institute of Cell Biology, University of Bern, Baltzerstrasse 4, Bern 3012, Switzerland.

[2]Present address: Max Planck Institute for Biology of Ageing, 50931 Köln, Germany.

Corresponding author: beat.suter@izb.unibe.ch

Keywords: aminoacyl tRNA synthetase, Su(H), Notch signaling, JAK/STAT signaling, stem cell, differentiation, proliferation, intestinal tumor

Author contributions: T.H., J.L., and B.S. conceived the ideas and designed the experiments. P.V.P and B.S. provided repeatedly input into the project development and they and J.L. performed and evaluated some experiments. T.H. conducted most experiments and performed the analysis of the results. T.H., J.L., and B.S. wrote the manuscript.

Abstract

The alpha subunit of the cytoplasmic Phenylalanyl tRNA synthetase (α-PheRS, FARSA in humans) displays cell growth and proliferation activities and its elevated levels can induce cell fate changes and tumor-like phenotypes that do neither dependent on the canonical function of charging $tRNA^{Phe}$ with phenylalanine nor on stimulating general translation. In intestinal stem cells of *Drosophila* midguts, α-PheRS levels are naturally slightly elevated and human *FARSA* mRNA levels are elevated in multiple cancers. In the *Drosophila* midgut model, elevated α-PheRS levels caused the accumulation of many additional proliferating cells resembling intestinal stem cells (ISCs) and enteroblasts (EBs). This phenotype resembles partially the tumor-like phenotype described as *Notch* RNAi phenotype for the same cells. Genetic interactions between *α-PheRS* and *Notch* suggest that their activities neutralize each other and that elevated α-PheRS levels attenuate Notch signaling whether Notch induces differentiation into enterocytes, neuroblast stem cell proliferation, or transcription of a Notch reporter. These non-canonical functions all map to the N-terminal part of α-PheRS which accumulates naturally in the intestine. This truncated version of α-PheRS (α-S) also localizes to nuclei and displays weak sequence similarity to the Notch intracellular domain (NICD), suggesting that α-S might compete with the NICD for binding to a common target. Supporting this hypothesis, the tryptophan (W) residue reported to be key for the interaction between the NICD and the Su(H) BTD domain is not only conserved in α-PheRS and α-S, but also essential for attenuating Notch signaling.

Author **Summary**

Aminoacyl tRNA synthetases charge tRNAs with their cognate amino acid to ensure proper decoding of the genetic code during translation. Independent of its aminoacylation function, the alpha subunit of *Drosophila* cytoplasmic Phenylalanyl tRNA synthetase (α-PheRS, FARSA in humans) has an additional activity that promotes growth and proliferation (Ho et al., 2021). Here we describe that elevated α-PheRS levels also induce cell fate changes and tumorous phenotypes in *Drosophila* midguts. Excessive proliferating cells with stem and progenitor cell characteristics accumulate and the composition of the terminally differentiated cells changes, too. This phenotype together with observed genetic interactions between α-PheRS and Notch levels show that α-PheRS counteracts Notch signaling in many different tissues and developmental stages. This novel activity of α-PheRS maps to its N-terminal part, which is naturally produced. The fragment contains a DNA binding domain, translocates into nuclei, and displays essential similarities to a Notch domain that binds to the downstream transcription factor. This suggests that it might be competing with Notch for binding to a common target. Not only because Notch plays important roles in many tumors, but also because *FARSA* mRNA levels are considerably upregulated in many tumors, this novel activity deserves more attention for cancer research.

71 # Introduction

72 Aminoacyl-tRNA synthetases (aaRSs) are essential enzymes that act by charging transfer
73 RNAs (tRNAs) with their cognate amino acid, a key process for protein synthesis (Schimmel
74 and Soll, 1979). Besides their well-known role in translation, aaRSs perform additional
75 functions in the cytoplasm, the nucleus, and even outside of the cell (Guo and Schimmel, 2013;
76 Nathanson and Deutscher, 2000; Smirnova et al., 2012) (Lee et al., 2004) (Casas-Tinto et al.,
77 2015; Gomard-Mennesson et al., 2007; Greenberg et al., 2008; Otani et al., 2002; Zhou et al.,
78 2014). Phenylalanyl-tRNA synthetase (PheRS, FARS, or FRS) displays elevated expression
79 levels in many cancers compared to their healthy counterparts according to the database "Gene
80 Expression across Normal and Tumor tissue" (GENT2; (Park et al., 2019)). Such a correlation
81 had been reported already two decades earlier and it was suggested that an alternative activity
82 of PheRS might contribute to the tumorigenic events (Sen et al., 1997) (Rodova et al., 1999).
83 A moonlighting function of the α subunit of *Drosophila* PheRS has recently been found to
84 promote growth and proliferation in different tissues (Ho et al., 2021). Despite this, a possible
85 mechanism explaining the connection between elevated PheRS levels and tumor formation had
86 so far not been reported and, to our knowledge, also not been studied.

87 Cytoplasmic PheRS is the most complex member of the aaRSs family, a
88 heterotetrameric protein consisting of 2 alpha- (α) and 2 beta- (β) subunits responsible for
89 charging $tRNA^{Phe}$ for translation (Roy and Ibba, 2006). The α subunit includes the catalytic
90 core of the tRNA synthetase and the β subunit has structural modules with a wide range of
91 functions, including tRNA anticodon binding, hydrolyzing misactivated amino acids, and
92 editing misaminoacylated $tRNA^{Phe}$ species (Ling et al., 2007; Lu et al., 2014; Roy and Ibba,
93 2006). Importantly, both subunits are needed for aminoacylation of $tRNA^{Phe}$.

94 We set out to address the question of whether and how the elevated levels of α–PheRS
95 that induce growth and proliferation (Ho et al., 2021) might contribute to tumor formation. To
96 test for this activity, we studied the role of α–PheRS levels in the *Drosophila* model system,
97 in which dissecting the molecular mechanism of such a moonlighting role of *α–PheRS* seemed
98 feasible. Tissue growth and homeostasis play important roles in developing and outgrown
99 animals, and they require tight control of stem cell self-renewal and differentiation into
100 daughter cells. The *Drosophila* midgut is a powerful model to analyze these mechanisms and
101 their interplay. Adult intestinal stem cells (ISCs) and adult midgut progenitors (AMPs) in the
102 larval gut can either divide asymmetrically or symmetrically (Jiang and Edgar, 2011; Micchelli,
103 2012). Asymmetric divisions of ISCs give rise to a new ISC and a Su(H)GBE$^+$ enteroblast (EB)
104 for the enterocyte (EC) lineage differentiation, or a pre-enteroendocrine cell (pre-EE) for the
105 enteroendocrine (EE) cell lineage differentiation (Furriols and Bray, 2001; Guo et al., 2016).
106 Differential Delta/Notch signaling between the ISC and its daughter causes the latter to either
107 differentiate into an absorptive EC lineage or a secretory EE lineage by distinct mechanisms
108 (Beehler-Evans and Micchelli, 2015; Micchelli and Perrimon, 2006; Ohlstein and Spradling,
109 2007; Zeng and Hou, 2015). EBs are intermediate differentiating cells that differentiate into
110 ECs in a Notch-dependent manner (Ohlstein and Spradling, 2006), while the production of EEs
111 has not been molecularly characterized. However, the pre-EEs require only low levels of Notch
112 signaling to differentiate into EEs (Guo *et al.*, 2016). Intestinal homeostasis is an interesting
113 system to elucidate the control of continuous replenishment of lost cells and the maintenance
114 of stem cells. Additionally, it turned out to be also a very dynamic process that can react to the
115 loss of large numbers of differentiated cells in response to injuries and bacterial infections.

116 We found that in different tissues and cell types, α-PheRS levels in stem and progenitor
117 cells regulate cell proliferation, cell differentiation, or both. Interestingly, a proteolytic α-
118 PheRS fragment that can neither interact with β-PheRS nor perform aminoacylation, promotes

these growth, proliferation, and differentiation functions. Although the consequences of altered levels vary to some degree between tissues, we found that even in tissues with the most divergent consequences, α-PheRS levels act by attenuating Notch signaling. Sequence comparisons combined with genetic and biochemical tests, as well as the cellular localization of this truncated α-PheRS (α-S) point to a mechanism whereby the N-terminal "DNA binding domain" of α-PheRS might compete with the NICD for the binding to a common target.

125 # Results

126 **PheRS is enriched in *Drosophila* gut stem cells**

127 PheRS promotes growth and proliferation in different tissues (Ho et al., 2021). In the
128 *Drosophila* midgut, intestinal stem cells (ISCs) display very high proliferation rates (Nagy et
129 al., 2018) due to a high turnover of the cells with a nutrient absorption mission. In addition, the
130 GENT2 database also reports highly elevated PheRS levels in many malignant cells compared
131 to normal tissues, and among these are also intestinal cancers (Park *et al.*, 2019). To investigate
132 the role of PheRS in intestinal cells, we examined the PheRS expression levels in wild-type fly
133 guts. ISCs and AMPs are ideal to study the novel PheRS activity because they can both undergo
134 either symmetric or asymmetric divisions and differentiate to maintain the cell population in
135 the fly gut. We observed that adult midguts express naturally elevated levels of α-PheRS in the
136 diploid wild-type ISC/EB cells compared to the enterocytes in the same tissue (Fig 1 A-A", B).
137 Similarly, a Myc-tagged α-PheRS under the normal genomic *α-PheRS* promoter is expressed
138 at higher levels in AMPs than in enterocytes of larval guts (Fig 1 C-C", D). To compare the
139 natural levels of α-PheRS in different cell types of the adult midgut, we used the *esg-Gal4*, *tub-*
140 *Gal80^{ts}*, *UAS-2XeYFP* system (hereby we refer as esg^{ts}) to label ISCs and EBs (Micchelli and
141 Perrimon, 2006) and Prospero staining to label enteroendocrine cells (EEs). This setup revealed
142 elevated expression of endogenous α-PheRS in YFP^{+} progenitor cells and EEs (Pros^{+}) than in
143 enterocytes (ECs; Fig 1E-F"").

144

145 **Elevated α-PheRS levels promote ISC and EE accumulation and altered EB morphology**

146 We previously constructed a mutant *α-PheRS* gene, that encodes an aminoacylation-dead
147 subunit (*α-PheRS^{Cys}*) that still displays the non-canonical activity of promoting growth and
148 proliferation (Ho et al., 2021). This mutant allows us to specifically study the activities of *α-*

149 *PheRS* that are not dependent on the aminoacyl tRNA synthetase activity of PheRS. To
150 investigate the effect of elevated levels of α-PheRS and α-PheRS^{Cys} (α-PheRS$^{(Cys)}$) on adult
151 midgut ISCs and EBs, we used *α-PheRS$^{(Cys)}$* under UAS control together with the esg^{ts} driver
152 system(Micchelli and Perrimon, 2006). Co-expression of *UAS-2XEYFP* allowed us to monitor
153 the activity of the *esg-Gal4* driver and to label ISCs and EBs. Upon controlled upregulation of
154 α-PheRS$^{(Cys)}$ levels, we observed two phenotypes in the intestines as early as 2 days after
155 induction and the phenotypes became more pronounced until day 5 (Fig S1). The first
156 phenotype resembled partially a *Notch* (*N*) knockdown-like phenotype with a 4.3 and 4.7-fold,
157 respectively, increase in the total numbers of YFP^{+} cells upon additional expression of α-PheRS
158 and α-PheRS^{Cys}, respectively (Fig 2A-C''', G). The increase of these midgut progenitor cells
159 (ISCs and EBs) could be a consequence of increased proliferation and/or a differentiation
160 problem of ISCs (Lian et al., 2018; Mundorf et al., 2019). Indeed, we also observed an increase
161 in the proportion of EEs from 8% in the control to 12% in the posterior midguts with elevated
162 *α-PheRS* expression (Fig 2H), indicating that elevated expression of *α-PheRS* promotes ISC
163 proliferation and EE accumulation.

164 The controlled upregulation of *α-PheRS$^{(Cys)}$* levels also led to a second phenotype, an
165 altered morphology of EBs. We observed a hyperaccumulation of YFP^{+} polyploid cells that
166 resembled the ones that have been referred to in other studies as "differentiating" EBs (Loza-
167 Coll et al., 2014; Zhai et al., 2017). Because these cells display ISC/EB characteristics (YFP^{+})
168 and EC characteristics (large polyploid nuclei) at the same time, it appears that they arrested
169 development between these two fates. Differentiating EBs were rarely observed in wild-type
170 midguts (3% of progenitor cells; Fig 2A-A''', I) and if they were present, they retained only
171 weak YFP signals. In midguts expressing elevated levels of α-PheRS$^{(Cys)}$, we observed much
172 higher levels of "differentiating" EBs (20% and 22%, respectively, of the YFP^{+} progenitor
173 cells), and these cells also displayed a strong YFP signal (Fig 2B-C''', I). We concluded that

174 the elevated levels of α-PheRS in the intestine induce hyperaccumulation of ISCs and EEs and
175 alterations in EB morphology.

176

177 **The phenotype of elevated α-PheRS levels partially resembles the low Notch phenotype**

178 Notch signaling is an important signaling pathway that coordinates ISC proliferation and
179 differentiation (Ohlstein and Spradling, 2006). We noted that the above-described changes
180 regarding ISCs and EEs partially overlapped with the low *N* activity phenotype that had been
181 reported in several studies (Guo and Ohlstein, 2015; Liu et al., 2010; Marianes and Spradling,
182 2013; Micchelli and Perrimon, 2006; Ohlstein and Spradling, 2007). To confirm this similarity,
183 we knocked down *N* with RNAi treatment with the same esg^{ts} system and this, indeed, led to a
184 typical phenotype in ISC proliferation and EE accumulation as reported in the studies
185 mentioned above (Fig 2D-D'''). This allowed us to compare the N^{RNAi} phenotype with the
186 phenotype of elevated $\alpha\text{-}PheRS^{(Cys)}$ levels (Fig 2B-C'''). The increase in YFP^{+} cells (290%;
187 from 27 to 104 cells) of N^{RNAi} treatment was in the same range as the one observed under
188 elevated *α-PheRS* expression (332%; from 27 to 115 cells), and with 12%, the proportion of
189 EEs was the same under the two conditions (Fig 2G, H). We also used the esg^{ts} driver to
190 upregulate Notch signaling by expressing the continuously active form of Notch, the Notch
191 intracellular domain (NICD). This caused ISCs to differentiate into ECs, thereby depleting 80%
192 of the ISC pool (Fig 2E-E''', G) and inhibiting EE differentiation (Fig 2E-E''', H) as it has been
193 reported in previous studies (Micchelli and Perrimon, 2006; Zhai *et al.*, 2017).

194 To test whether $\alpha\text{-PheRS}^{(Cys)}$ interferes with Notch signaling, we simultaneously
195 elevated levels of $\alpha\text{-}PheRS^{(Cys)}$ and NICD. This schema had a rescuing effect on both
196 phenotypes. On the one hand, it rescued the ISC pool and proportion of EEs depleted by NICD
197 expression even beyond the wild-type levels (Fig 2F-F''', G). On the other hand, the phenotype

198 caused by the additional expression of the NICD can also be interpreted as a partial rescue of
199 the phenotype caused by elevated α-PheRS$^{(Cys)}$ levels. The numbers of YFP^{+} cells and
200 differentiating EBs dropped considerably, even though they remained still higher than in the
201 wild type (Fig 2D-F''', G, I). These results suggest that the two phenotypes observed when *α-*
202 *PheRS*$^{(Cys)}$ expression was elevated in ISCs and EBs arise because *α-PheRS*$^{(Cys)}$ and Notch
203 signaling counteract each other for the control of proliferation and differentiation.

204 We next tested whether α-PheRS$^{(Cys)}$ can downregulate *Notch* signaling in adult
205 midguts using the *Notch* reporter NRE-eGFP (Notch response element promoter driving the
206 expression of eGFP; (Saj et al., 2010). As seen in Fig 2J, the expression of α-PheRS and α-
207 PheRS^{Cys} clearly reduced the *N*-driven expression of the N-signaling reporter. We conclude
208 that elevated α-PheRS levels in midgut stem cells cause misregulation of gut homeostasis and
209 that this effect is not only the consequence of the proliferative role of α-PheRS but also caused
210 by downregulating Notch signaling and inhibiting the terminal differentiation of the progenitor
211 cells (EBs).

212

213 **Elevated α-PheRS levels induce AMP proliferation and interfere with gut homeostasis**

214 Larval *Drosophila* midguts possess AMPs as the temporary reserve for adult ISCs. AMPs go
215 through several divisions to form imaginal midgut islets that consist of AMPs enclosed by
216 peripheral cells (PC) (Mathur et al., 2010). Due to the transient period of the larval stage, larval
217 midguts do not require EC renewal under normal conditions (Lee and Lee, 2019). However,
218 larval guts can respond to certain damages and injuries by triggering a regenerative process
219 that compensates for depleted ECs in the epithelium and also allows reconstituting the AMP
220 pool (Houtz et al., 2019). We also investigated the effect of elevated *α-PheRS* levels on larval
221 AMPs by using the *esg-Gal4, UAS-2XEYFP* driver, which is specifically expressed in AMPs.

222 Co-expression of *UAS-2XEYFP* allowed us to monitor the activity of the *esg-Gal4* driver and
223 to label AMPs. The results demonstrated that elevated Myc::α-PheRS in the larval midgut
224 significantly increased the proportion of EE and PH3 positive cells (mitotic cells) in the
225 posterior midgut (Fig 3A-D, I-K, L, M). This increased EE proportion again pointed out the
226 similarity with the Notch knockdown-like phenotype in the adult gut. Driving the expression
227 of α-PheRS^{Cys} in AMPs also produced a higher mitotic index (Fig 3E-F, L), indicating that the
228 aminoacylation function is not required for this activity. Due to the lack of epithelial renewal
229 in normal larval guts, the cell density of larval midguts is usually stable (Lee and Lee, 2019;
230 Mathur *et al.*, 2010). It is therefore surprising that elevated α-PheRS$^{(Cys)}$ levels increase the cell
231 density in larval midguts (Fig 3N). Altogether, these results show that elevated α-PheRS$^{(Cys)}$
232 levels cause AMPs to proliferate and to differentiate, producing additional larval midgut cells.

233 Strikingly, elevated α-PheRS^{Cys} levels induced tumor-like phenotypes in both anterior
234 and posterior areas of the larval midgut (outlined with white dashed lines, Fig 3E-F) while the
235 elevation of wild-type Myc::α-PheRS only gave rise to high numbers of AMPs in the posterior
236 larval midgut (Fig 3C,D). Elevated α-PheRS^{Cys} levels also caused the appearance of a more
237 severe tumor-like phenotype, where individual AMP islets could not be discerned anymore
238 (Fig 3E-F). Wild-type larval guts contain ECs with large nuclei and interspersed occasional
239 AMP islets with smaller nuclei (as seen in the YFP overexpression control, Fig 3A-B). In
240 contrast, we observed a phenotype where ECs and AMPs could not be distinguished based on
241 the size of their nuclei but emerged as a larger cell population with intermediate size nuclei
242 (Fig 3D). Many of these cells expressed the *esg*>YFP stem cell marker at high levels, but others
243 displayed only a very weak YFP signal. This result is comparable to the EB phenotype in adult
244 midguts where the progenitor cells remain in an intermediate differentiation state (Fig 2B"',
245 C"'). Notably, this phenotype was also observed when Notch was downregulated by RNAi

246 using the same induction system (Fig 3G-H). This points again to the possibility that
247 downregulation of Notch signaling is involved in producing this phenotype.

248

249 ***α-PheRS* is a novel general repressor of Notch signaling**

250 Developing larval brains contain neuroblasts (NBs), neuronal stem cells that divide
251 asymmetrically with one daughter keeping the stemness and the other differentiating into a
252 neuronal cell. Notch signaling plays a crucial role in this process (Ables et al., 2011; Giachino
253 and Taylor, 2014), but in contrast to the situation in the gut, loss of *Notch* prevents NB self-
254 renewal, whereas ectopic expression of activated Notch leads to tumor formation (de la Pompa
255 et al., 1997; Grandbarbe et al., 2003; Hatakeyama et al., 2004). This opposite role of *Notch*
256 makes the NB lineage an ideal complementary system to test whether α-PheRS is a general
257 component of the *Notch* pathway. Driving α-PheRS or the α-PheRS^{Cys} expression in NBs with
258 the *inscutable-Gal4 (incs-Gal4)* driver resulted in significantly smaller central brains (CB), the
259 region where the type I and II NBs are located (Fig 4A-C, G). In contrast, this treatment had
260 little or no effect on the size of the optic lobes (OL). Importantly, the phenotype was virtually
261 indistinguishable from the phenotype caused by *N* knock-down (Fig 4E), although the
262 phenotype of the latter might show slightly higher expressivity. Analogous to the situation in
263 the gut, co-expression of NICD together with *α-PheRS^{Cys}* in neuroblasts rescued the brains to
264 wild-type size (Fig 4D,G).

265 Type II neuroblasts are particularly suited to analyze effects on neuroblast
266 differentiation. Targeting specifically the eight type II neuroblasts in central brain lobes with
267 ectopic *α-PheRS* or *α-PheRS^{Cys}* expression, resulted in a strong reduction of the number of type
268 II neuroblasts (Fig 4H-M, N). Knocking down *Notch* in type II NBs with RNAi and the same
269 driver combination resulted in a similar phenotype, but with a higher expressivity (Fig 4K). On

270 the other hand, overexpression of α-PheRS in type II neuroblasts where Notch signaling was
271 also over-activated by the co-expression of NICD (Fig 4M) partially rescued the tumor
272 phenotype of type II neuroblasts to wild-type numbers and it restored the normal size of the
273 brain (Fig 4L). Because the genetic interaction with *Notch* shows that the two activities
274 counteract one another in guts and brains, two tissues where *Notch* has opposing functions on
275 cellular differentiation, it appears that the interaction between *α-PheRS* and *Notch* is not
276 mediated indirectly through a primary effect on division or differentiation but is likely to be a
277 more direct one. In any case, this interaction appears to modulate tissue homeostasis in different
278 organs.

279 To further address the role of *α-PheRS* on Notch signaling, we also studied its effect on
280 the larval wing disc and the adult wing. Using the *en-Gal4*, *tub-Gal80*^{ts} (referred to as en^{ts}
281 system) to elevate *α-PheRS* expression allowed us to specifically and conditionally activate *α-*
282 *PheRS*$^{(Cys)}$ expression in the posterior compartment of the wing disc by temperature-shift
283 control. Reduced Notch signaling in the posterior wing disc can cause the notched wing
284 phenotype at the distal end of the wing and the emergence of an ectopic partial vein in the
285 center of the posterior compartment. The additional expression of *α-PheRS*$^{(Cys)}$ in the posterior
286 compartment did not produce the distal phenotype and we will discuss possible reasons for this
287 in the Discussion. However, elevated *α-PheRS* or *α-PheRS*^{Cys} levels induced the central ectopic
288 vein phenotype also observed under low Notch signaling conditions (Fig S4A-D ; (Johannes
289 and Preiss, 2002). The new vein branches off from the connecting vein between the L4 and L5
290 vein (arrowhead, Fig S4B,C) and is indistinguishable from the one obtained by downregulating
291 *Notch* by RNAi treatment using the same expression system (Fig S4D). Again, these findings
292 suggest that *α-PheRS* might be a more general, novel regulator of Notch signaling.

293 To test directly for changes in *Notch* activity in response to altered levels of *α-*
294 *PheRS*$^{(Cys)}$ in imaginal wing discs, we monitored Notch activity with the NRE-eGFP reporter

295 and used the en^{ts} system together with *UAS-mRFP* to conditionally express *α-PheRS$^{(Cys)}$* in the
296 posterior compartment. In this system, eGFP expression marks the cells with active Notch
297 signaling, which normally localize along the dorsal-ventral (D/V) boundary of the larval wing
298 disc (Fig 5A"), and it marks the posterior, en-Gal4^{+}, compartment of the wing disc with mRFP,
299 allowing us to assess *N* activity in this compartment (black arrowhead, Fig 5A"') while using
300 the anterior compartment as the internal control. In wild-type wing discs, the NRE-eGFP signal
301 is as strong in the posterior compartment as in the anterior one (Fig 5B-B"'). Knockdown of
302 *Notch* in the posterior compartment resulted in the exclusion of the NRE-eGFP signal from the
303 mRFP-marked posterior compartment (white arrow, Fig 5E-E"'). Importantly, elevated *α-*
304 *PheRS$^{(Cys)}$* levels also caused a loss of the eGFP signal in the mRFP-marked posterior
305 compartments (Fig 5C-C"', D-D"'). These observations demonstrate that elevated *α-PheRS*
306 levels downregulate *Notch* activity in larval wing discs and that this inhibition acts on Notch
307 signaling at or before the transcription of the reporter. Taken together, the results from midguts,
308 brains, and wing discs demonstrate that *α-PheRS* is a novel general repressor of *Notch*
309 signaling.

310

311 **The N-terminal 200 amino acids of α-PheRS (α-S) are sufficient to induce the proliferative**
312 **phenotype and to repress Notch activity**

313 Having shown that the growth and proliferation function and the counteracting of the Notch
314 signaling are independent of the aminoacylation activity of α-PheRS, we wanted to find out
315 whether this activity can be separated from the catalytic domain. As shown in Fig 6A,B, the C-
316 terminal catalytic domain is separated by a linker region from the N-terminal part. We,
317 therefore, cloned the first 200 codons of the α-PheRS ORF under UAS control and added a
318 Myc tag at the beginning of the open reading frame, giving rise to the *UAS-Myc::α-S* (*α-S*)
319 gene (Fig 6B). Expressing *α-S* with the en-Gal4 driver and staining wing discs for Myc,

320 revealed that this truncated version of α-PheRS was stably expressed in the posterior wing disc
321 compartment (Fig S3). To test whether this C-terminally truncated isoform was able to repress
322 Notch signaling, too, we expressed *α-S* with the esg^{ts} driver in larval and adult guts and found
323 that it produced an excessive number of Esg^{+} cells (Fig 6C-C"', D-D"'), an increase in mitotic
324 cells (Fig 6F) and that it diverted ISC differentiation toward the EE fate (Fig 6E, E', G). The
325 truncated isoform α-S is capable of inducing the production of many cells with stem cell
326 characteristics and it directs their differentiation towards an EE fate, just like α-PheRS$^{(Cys)}$ does.
327 Similarly, expressing *α-S* in the posterior compartment of wing discs induced ectopic vein
328 formation between the L4 and L5 veins in the adult wing (Fig S4E-F) and the same loss of the
329 Notch reporter signal (NRE-eGFP) in the posterior compartments of wing discs as full-length
330 *α-PheRS$^{(Cys)}$* did (Fig 6H-I'). These observations demonstrate that elevated *α-S* levels
331 downregulate *Notch,* mapping the inhibitory activity to the N-terminal 200 amino acids.

332 Expressing transgenic Myc::α-PheRS under the control of the *Tub-Gal4* driver revealed
333 beside the full-length α-PheRS isoform (55kDa) also one stable isoform around 40 KDa and
334 another around 25KDa (Fig 6J). To study the expression pattern of these isoforms, we dissected
335 different larval tissues and found that the 40 KDa isoform was present in larval heads and fat
336 bodies, while larval guts showed predominantly the 25 KDa isoform (Fig 6K). The 25 KDa
337 isoform might either arise if Myc::α-PheRS is cleaved in the linker domain or if the pre-mRNA
338 is processed in a different way to give rise to a shorter, but stable isoform. Because there is no
339 evidence for alternatively processed mRNAs of α-PheRS in wild-type animals (flybase.org
340 version FB2019_04; (Thurmond et al., 2019), we tested whether PheRS might get cleaved *in*
341 *vivo* to produce an isoform that resembles Myc::α-S. Myc-tagged isoforms were isolated from
342 total larvae by immunoprecipitation and gel purification, and their polypeptides were identified
343 by mass spectrometry (MS). The MS data shows the peptide coverage of the 25KDa isoform
344 according to the score of Peptide Spectrum Matches (PSM; Fig S2). The 25 KDa isoform

345 contains the peptides of the N-terminal 28% of the full-length α-PheRS. Even though we
346 identified two more C-terminal peptides, which could not be rejected based on the PSM
347 interpretations, these two peptides were likely recovered due to a "memory effect" of the
348 column. This indicates that the 25 KDa isoform is a C-terminally truncated version of α-PheRS
349 that strongly resembles the α-S that performs the non-canonical functions.

350

351 **Mechanism of downregulating Notch signaling by α-S**

352 Given the competitive interaction between *α-PheRS* and *Notch* and the effect of the α-S isoform
353 on downregulating N activity, we aligned the polypeptide sequence of α-S and Notch, and this
354 revealed similarities between α-S and the RAM domain (RBP-Jκ-associated molecule) of
355 Notch (Fig 7A). To transmit the Notch activity, the RAM domain of the NICD binds through
356 the tetra-peptide motif ΦWΦP to the beta-trefoil domain (BTD) of Suppressor of Hairless
357 (Su(H)), the *Drosophila* CSL/RBPJ. This allows the complex to interact with specific DNA
358 sequences in the promoter region of the target genes to activate transcription (Barrick and
359 Kopan, 2006; Borggrefe and Oswald, 2009; 2016; Gordon et al., 2008; Kovall, 2007).
360 Mammals can repress Notch activity with proteins containing the tetra-peptide motif ΦWΦP.
361 These compete with NICD to bind to CSL/RBPJ and form the Complex of Repressor (CoR)
362 that inhibits Notch target gene activation (Bray and Furriols, 2001; Fortini and Artavanis-
363 Tsakonas, 1994; Nagel et al., 2017; Praxenthaler et al., 2017). Even though the tetrapeptide is
364 only partially conserved in α-S, the similarities between α-S and the RAM domain of Notch,
365 and the presence of the tryptophan residue (W) flanked by Φ (Fig 7A) led us to hypothesize
366 that α-S and NICD might compete for a common target.

367 To test this hypothesis, we mutated the conserved "W" (tryptophane) codon in *α-S* to
368 give rise to *Myc::α-S*^{W112A} and analyzed the effect of this mutation on Notch signaling in vivo.
369 To test whether the mutation W112A does not affect the stability of the *α-S* polypeptide, we

370 used the en-Gal4 system to overexpress *Myc::α-S* and *Myc::α-S*^{W112A} and stained larval wing
371 discs with Myc antibodies. The mutant still showed a similar expression in the posterior
372 compartment of the wing discs as the wild-type α-S (Fig S3), confirming that the mutation does
373 not affect protein stability. In contrast to what was seen upon wild-type expression of α-PheRS
374 (Fig 2), expressing *Myc::α-S*^{W112A} with the esg^{ts} driver in adult guts did neither induce the
375 overproliferation phenotype (excessive numbers of Esg^{+} cells) nor the differentiation
376 phenotype (higher EE/EC ratio) (Fig 7B, C, G, H). These results could also be confirmed when
377 a full-length version of *α-PheRS* with the mutation W112A was expressed with the same driver
378 (Fig 7D, G, H). To further test whether α-PheRS with the W112A mutation lost its ability to
379 interfere with Notch signaling, we simultaneously elevated levels of Myc::α-S^{W112A} or α-
380 PheRS^{W112A} together with NICD levels. Indeed, the mutated Myc::α-S^{W112A} or α-PheRS^{W112A}
381 did not rescue the ISC pool or the EEs, the two cell types that are depleted by NICD over-
382 expression (Fig 7F-F"', G, H). Furthermore, because a genomic construct expressing this
383 mutant version of *α-PheRS*^{W112A} *(gα-PheRS*^{W112A}*)* under its native promoter rescued the *α-*
384 *PheRS* null mutant, the W112A mutation does not prevent the canonical activity of *α-PheRS*
385 and produces sufficient protein that can perform the aminoacylation reaction. This also shows
386 again that this mutant protein is stable.

387 NICD is known to enter the nucleus the perform its function in transcriptional control.
388 To test whether α-S is also able to enter the nuclei, we use the esg^{ts} system to drive Myc::α-S
389 expression and stained guts for Myc. As shown in Fig 7I-I"' and K (compare to Fig 1B,D), we
390 found high levels of Myc::α-S signal in nuclei of progenitor cells (YFP^{+} cells), revealing that
391 α-S can translocate to nuclei. Similarly, the Myc::α-S^{W112A} signal was also present in nuclei of
392 YFP^{+} cells (Fig 7J-J"',L), indicating that the W112A mutation neither affects stability nor
393 translocation into nuclei. These results, therefore, show that W^{112} in α-PheRS plays an
394 important role in counteracting Notch signaling in ISCs and EBs.

395 # Discussion

396 Notch signaling regulates diverse cellular behaviors during tissue growth in a context-
397 dependent manner. Most prominently, these are proliferation and differentiation (Henrique and
398 Schweisguth, 2019; Hori et al., 2013). In this study, we presented the effect of α-PheRS on
399 downregulating Notch signaling activity in different tissues where Notch induces diverse
400 outcomes. In the larval brain, Notch signaling promotes NB self-renewal, and ectopic
401 expression of NICD leads to tumor formation (de la Pompa *et al.*, 1997; Grandbarbe *et al.*,
402 2003; Hatakeyama *et al.*, 2004). Here, elevated α-PheRS showed an inhibitory effect on Notch
403 signaling, preventing NB self-renewal and thereby reducing the size of the brain lobe (Fig 4A-
404 A",B). Accordingly, elevated α-PheRS in this situation also rescued the tumor phenotype
405 caused by the expression of the activated form of Notch, NICD (Fig 3 G,H). Also in this
406 situation, expressing only the N-terminal part of α-PheRS, the region that does not contain any
407 catalytic domains and that does not interact with the β-PheRS subunit (Fig 6C; (Finarov et al.,
408 2010) was just as effective in producing the same phenotypes as α-PheRS$^{(Cys)}$.

409 In the intestine, the regulation of Notch is crucial for ISC fate decisions. Any
410 interference with this signaling pathway alters the composition of the gut cell population. We
411 found that even modest elevation of the levels of the essential cellular household enzyme α-
412 PheRS drastically changed the composition of the intestinal cell population. Aside from
413 hyperaccumulation of ISCs, EE cells and "differentiating EBs" become more abundant. This
414 phenotype has also been reported in the studies by Korzelius and colleagues (Korzelius et al.,
415 2019; Korzelius et al., 2014). They reported that the WT1-like transcription factor Klumpfuss
416 (Klu) is regulated by Notch signaling and maintains the lineage commitment of enterocyte
417 progenitors in the *Drosophila* intestine. Similar as elevated α-PheRS levels, loss of *klu* function
418 also leads to blockage of EC differentiation, causing the "differentiating EB" phenotype and

419 diverting EBs into EE differentiation. Because Notch signaling has been reported to regulate
420 *klu*, it appears that α-PheRS levels also act upstream of *klu*.

421 Elevated levels of α-PheRS reproduced the "vein formation" phenotype in the adult
422 wings caused by loss-of-Notch (Fig 6A-A"') (Johannes and Preiss, 2002), and these increased
423 levels also prevented the transcription of the Notch transcriptional reporter NRE-eGFP at the
424 D/V boundary of larval wing discs (Fig 6D-E"'). This inhibition of Notch signaling must
425 therefore happen at or before the transcription of the reporter. Reminiscent of its function in
426 neuroblasts, Notch signaling at the D/V boundary region of the wing disc promotes
427 proliferation (de Celis et al., 1996). Upon additional expression of α-PheRS in this region, not
428 only Notch activity (Fig 5), but also $PH3^+$ cells became absent from this region (Ho et al.,
429 2021). Interestingly, however, in regions of the posterior wing disc compartment where there
430 is no Notch activity, elevated α-PheRS caused the appearance of additional $pH3^+$ cells (Ho et
431 al., 2021). Because knockdown of *N* causes the notched wing phenotype but increased α-
432 PheRS levels do not (Fig 6A), it would be interesting to find out whether the proliferation of
433 these additional $pH3^+$ cells that reside outside of the region with *Notch* activity can compensate
434 for the cells along the D/V boundary that depend on Notch signaling to be mitotically active.
435 We do not know yet how elevated α-PheRS levels induce this cell proliferation, but an effect
436 on the organ size control pathway Hippo signaling might be a candidate. On the other hand,
437 the complexity of the Notch signaling at the D/V boundary, where downregulation or
438 overactivation of Su(H) can cause indistinguishable phenotypes (Furriols and Bray, 2000)
439 makes conclusions difficult. Furthermore, cell proliferation in the distal wing margin is
440 regulated also by epidermal growth factor (EGF) or decapentaplegic (Dpp)/bone
441 morphogenetic protein (BMP) signaling (Biehs et al., 1998; Teleman and Cohen, 2000)
442 (Shimmi et al., 2014), suggesting that interactions with other signaling mechanisms might be
443 involved, too. In any case, we conclude that even in the wing, α-PheRS represses Notch

signaling, but different regions of the wing disc respond differently to α-PheRS levels, making the wing disc a more complex system to study the responses to elevated α-PheRS levels.

In ovarian follicle cells, the elevated levels of α-PheRS led to an increase in clone size with more cells per clone (Ho et al., 2021). This could possibly also be caused by an inhibitory effect of α-PheRS on Notch signaling because Notch is required for the follicle cells to exit the mitotic cycle and switch to the endocycle (Lopez-Schier and St Johnston, 2001) and loss of Notch signaling prevents the epithelial cells from switching from the mitotic cell cycle to the endocycle, leading to over-proliferation of follicle cells (Deng et al., 2001; Shcherbata et al., 2004). Similarly, in adult midguts, elevated α-PheRS interfered with normal homeostasis of ISCs by inducing a typical low Notch signaling phenotype with many more ISCs, EBs, and EEs (Micchelli and Perrimon, 2006; Ohlstein and Spradling, 2007; Zhai et al., 2015). Because α-PheRS levels attenuate Notch signaling in different situations where Notch causes diverse effects, α-PheRS (or a part of it) seems to be a general component of the *Drosophila* Notch signaling pathway.

Repression of Notch signaling through competition with the NICD has been described in different systems and has recently been reviewed (Maier, 2019; Oswald and Kovall, 2018). Best studied is probably the competition involving the factors binding to the C-terminal domain (CTD) of Su(H) (CSL in vertebrates and RBPJ in mammals) that lead to the formation of the Complex of Repressor (CoR) that inhibits Notch target gene activation. A less well-studied group of competitors compete directly with the binding of the RAM domain of the NICD to the BTD of the Su(H) ortholog CSL/RBPJ (Maier, 2019; Oswald and Kovall, 2018). This competition involves the 20 N-terminal amino acids of the RAM domain, which contain the hydrophobic tetrapeptide with the key tryptophane residue (ΦWΦP). So far, this competition was only seen in mammals and, therefore, considered to be specific for vertebrate Notch

468 signaling. Known competitors are Epstein-Barr nuclear antigen 2 (EBNA2), mouse
469 KyoT2/FHL1, and human RITA (RBPJ interacting and tubulin associated) (Collins et al., 2014;
470 Johnson et al., 2010; Tabaja et al., 2017; Taniguchi et al., 1998; Wacker et al., 2011; Zimber-
471 Strobl and Strobl, 2001). Based on our results, a naturally occurring fragment of the α-PheRS
472 household protein might function through this mechanism to modulate or attenuate Notch
473 signaling if this invariant W is present. The immediately adjacent hydrophobic residues are
474 also present in the α-S tetrapeptide sequence. However, the residue in position four, a proline,
475 is substituted by another hydrophobic residue, leucine. Interestingly, even in mammals, this
476 residue is less conserved than the W in position two (Maier, 2019). Two additional elements
477 have been discussed to affect the affinity of the interaction between the RAM domain and the
478 transcription factor (CSL, RBPJ, or Su(H)) (Oswald and Kovall, 2018). The dipeptides -HG–
479 and –GF–. Interestingly, both dipeptides are also present in the N-terminal 20 amino acids of
480 the RAM domain of *Drosophila* Notch, α-PheRS, and α-S even though they are found in
481 different positions (Fig 7A). Their contribution to the binding affinity would therefore have to
482 be further evaluated. Additionally, the α-S polypeptide also contains a KKRK sequence
483 element that might function as a nuclear localization sequence (NLS). It could therefore allow
484 α-S to actively enter the nucleus to bind to a partner (Fig 7I-I"'). Notably, α-PheRS$^{(Cys)}$ is a
485 cytoplasmic protein for which we did not observe clear nuclear localization (Fig 1B,D). This
486 might suggest that processing or truncation of α-PheRS$^{(Cys)}$ facilities the translocation of its
487 signaling domain α-S into nuclei, a process that might even play an important role in fine-
488 tuning of this novel α-PheRS activity. This model is also consistent with the result that α-PheRS
489 and α-S act on Notch signaling at or before the transcription from the Nre element of the Nre-
490 eGFP reporter and, finally, an α-S activity in transcriptional control could also shed light on
491 the puzzling question of why a cytoplasmic aaRS contains a DNA binding domain (Abul et al.,
492 2001, Na Wei et al., 2014). However, at least until *in vivo* binding of α-S to Su(H) is

493 demonstrated, other competitions with Notch still need to be considered. Furthermore, because
494 α-S also displays proliferative activities that seem not to be mediated by its effect on Notch
495 signaling, we expect that α-S or its downstream targets act also on components of other
496 signaling pathways, like for instance the organ size control pathway.

497 A correlation between elevated levels of α-PheRS/FARSA and tumor formation has
498 been noted some time ago (Sen *et al.*, 1997) and is also suggested by the data published in the
499 GENT2 database (Park *et al.*, 2019). Not the least because colon cancers are among the ones
500 that express higher levels of α-PheRS in the tumor tissue than in the healthy counterpart,
501 modeling the effect of elevated α-PheRS levels in *Drosophila* ISCs and EBs might reveal
502 mechanisms contributing to tumor development. In the gut tissue, elevated α-PheRS and α-
503 PheRS^{Cys} levels produced 12-14 times as many tumors and these showed mostly a more severe
504 phenotype (Fig 3H). Such tumors were composed of ISCs and differentiating EBs. Similarly,
505 guts also contained 5-8 times as many mitotic cells when α-PheRS$^{(Cys)}$ levels were elevated
506 (Fig 3E). Together, these results strongly suggest that higher levels of α-PheRS can induce
507 strong cell proliferation. Additionally, because these over-proliferation cells display stem cell
508 characteristics and changes in cell fate, elevated α-PheRS levels might be a risk factor for
509 tumor formation.

510 The hyperaccumulation of cells with stem cell characteristics is mediated by high α-
511 PheRS$^{(Cys)}$ or α-S repressing Notch signaling and possibly affecting also another signaling
512 pathway. In mammals, Notch signaling is essential for maintaining the homeostasis of cell
513 proliferation and differentiation (Qiao and Wong, 2009) similar to the function of Notch
514 signaling in the *Drosophila* gut that is needed to prevent the induction of tumors in the adult
515 midgut (Micchelli and Perrimon, 2006; Ohlstein and Spradling, 2007). In humans,
516 misregulation of Notch signaling in these processes has been suggested to trigger the

517 development of colon cancer, and *Notch* has been proposed as a molecular target for cancer
518 therapy (Yin et al., 2010). Furthermore, several other tumors contain low Notch levels and
519 elevated α-PheRS/FARSA levels (Park *et al.*, 2019). Amongst them are for instance skin, head
520 and neck, soft tissue, muscle, and tongue tumors. In these cases, it would be interesting to find
521 out whether elevated FARSA levels cause the downregulation of Notch. Notch signaling has
522 been found inactivated in different squamous cell carcinoma, including cutaneous, head and
523 neck, and esophageal squamous cell carcinoma, and also in small-cell lung cancers (ScLc)
524 (Katho and Katho, 2020). However, Notch signaling in tumors is more complex because Notch
525 acts intrinsically both tumor suppressive and oncogenic. The latter has been observed in some
526 subtypes of gastric and esophageal cancers, colorectal cancer, uterine corpus endometrial
527 cancer, breast cancer, and non-small-cell-lung cancer (Katho and Katho, 2020). A more in-
528 depth analysis of the relationship between FARSA levels and Notch activity should therefore
529 also consider that elevated levels of FARSA might reflect a reaction of the cell to counteract
530 excessive Notch activity. The results presented here provide new and unexpected insights into
531 the regulation of Notch signaling in the context of gut tumorigenesis and they suggest new
532 opportunities to target these mechanisms.

533

534 # Materials and Methods

535 ## Key Resources Table

Reagent or Resource	Sources	Identifier	Additional information
Antibodies			
Anti phospho-Histone H3-rabbit	Cell signaling	9701S	1:200 v/v
Anti phospho-Histone H3-mouse	Cell signaling	9706S	1:200 v/v
Anti *α-PheRS*	Genescript	4668	Customized product (1:200 v/v)
Anti *α-PheRS*	Genescript	4669	Customized product (1:200 v/v)
Anti Myc-mouse	Developmental Studies Hybridoma Bank (DSHB)	9E10	Supernatant (1:3 v/v)
Anti Puromycin	DSHB	PMY-2A4	1:100 v/v
Anti Prospero	DSHB	MR1A	1:200 v/v
Anti Delta	DSHB	C594.9B	1:10 v/v
Anti V5 tag-rabbit	Cell signaling	13202	1:200 v/v
Anti Cy3 rabbit	Jackson Immuno Research	115-165-146	1:200 v/v
Anti-rabbit Alexa Flour 488	Molecular Probes	A-11008	1:200 v/v
Anti-rabbit Alexa Flour 488	Molecular Probes	A-11034	1:200 v/v
Anti-mouse Alexa Flour 488	Molecular Probes	A-11029	1:200 v/v
Anti-rabbit Alexa Flour 488	Life technology	A-21206	1:200 v/v
Anti-rabbit Alexa Flour 594	Invitrogen	A-11037	1:200 v/v
Anti-mouse Alexa Flour 594	Molecular Probes	A-11032	1:200 v/v
Anti-mouse Alexa Flour 568	Life technology	A-10037	1:200 v/v
Anti α-tubulin	Abcam	Ab18251	1:1,000 v/v
Anti GFP	ImmunoKontact	042704	1:1,000 v/v
Anti Myc-rabbit	Santa Cruz	Sc-789	A-12 (1:1,000 v/v)
HRP anti-rabbit IgG antibody (Peroxidase)	Vector	PI-1000	1:10,000 v/v
HRP anti-rabbit IgG antibody (Peroxidase)	Vector	PI-2000	1:10,000 v/v

536

Fly stocks and genetics			
α-PheRS^{G2060}/FM6	Bloomington *Drosophila* Stock Center (BDSC)	26625	
gα-PheRS^{Cys}			Transgenic construct
UAS-α-PheRS^{Cys}			Transgenic construct
hspFLP; Act-Gal4/CyO; neoFRT82B, tub-Gal80/TM3, Sb			
w; If/CyO; neoFRT82B, UAS-α-PheRS$^{(Cys)}$			
engrailed-Gal4	BDSC	30564	
engrailed-Gal4, NRE-EGFP, UAS-myrRFP	BDSC	30730	
UAS-GFP	BDSC	6658	
w; UAS-Myc::MYC	BDSC	9674	
hspFLP/y; +; UAS-Myc::MYC	BDSC	9675	
hspFLP/y; UAS-NICD /CyO; MKRS/TM2	BDSC	52008	
NRE-EGFP	BDSC	30727	
UAS-N RNAi	BDSC	7078	
*neoFRT*82B *Sb1*/TM6	BDSC	2051	
NRE-eGFP	BDSC	30728	
UAS-Dl	BDSC	5614	
tub-Gal4/TM3, Sb	BDSC	5138	
w*, Insc-Gal4	BDSC	8751	
w*, UAS-Dicer2; wor-Gal4, ase-Gal80; UAS-mCD8::GFP	IMBA		A gift from Juergen A. Knoblich, IMBA
y w att2A[vas-ϕ]; +; attP-86F	ETH Zurich		A gift from Hugo Stocker, ETH
esg-Gal4, UAS-2XEYFP; MKRS/TM6B, Tb	ETH Zurich		A gift from Hugo Stocker, ETH
esg-Gal4, UAS-2XEYFP; tub-Gal80^{ts}/TM3, Sb	ETH Zurich		A gift from Hugo Stocker, ETH
yw; esg-Gal4, UAS-GFP/TM6B, Tb, Hu	ETH Zurich	2400	A gift from Hugo Stocker, ETH
NP1-Gal4 (Myo31DF or Myo1A-Gal4)/CyO, y+	ETH Zurich	2398	A gift from Hugo Stocker, ETH
esg-Gal4, UAS-mCherry-CD8, tub-gal80^{ts}/CyO			A gift from Péter Nagy, Cornell University
yw;UAS-cyto-gars-myc/CyO			A gift from Albena Jordanova, VIB-U Antwerp Center for Molecular Neurology

537

538

Bacteria strains and vectors		
XL1 blue	Aligent	200249
Rosetta – Novagen	Merck milipore	70954
pET-28a – Novagen	Merck milipore	69864
pET LIC (2A-T)	Addgene	29665
pUASattB	*Drosophila* Genomics Resource Center	1419
pw+SNattB	(Koch et al., 2009)	
Commercial assay or kit		
Pierce Silver Stain kit	Thermo Scientific	24612
Pierce BCA Protein Assay kit	Thermo Scientific	23227
ReliaPrep DNA CleanUp and Concentration System	Promega	A2893
GeneElute HP Plasmid miniprep kit	Sigma	NA0160
Qiagen Plasmid Plus Midi kit	Qiagen	12943
Ni-NTA affinity resin	Qiagen	30210
ECL Prime Western Blotting System	GE Healthcare	RPN2232
RNAMaxx High Yield Transcription Kit	Agilent	200339
Software, algorithm		
Leica Application Suite X (LAS X)	Leica	https://www.leica-microsystems.com/products/microscope-software/p/leica-las-x-ls/
FIJI	ImageJ	https://fiji.sc/
GraphPad Prism	GraphPad	https://www.graphpad.com/scientific-software/prism/
FlowJo	BD Biosciences	https://www.flowjo.com/
Microsoft Excel	Microsoft	https://products.office.com/en-us/excel

539

540 **Buffers**

Lysis buffer for *Drosophila* tissue	**Lysis buffer for bacteria**
20 mM Tris HCl pH7.4 150uM NaCl 2 mM EDTA 50 mM NaF 10% Glycerol 1% Triton X100 1 Protease inhibitor cocktail tablet (Roche-4693159001) 1 mM phenylmethylsulphonyl fluoride	20 mM Tris HCl pH7.4 150uM NaCl 2 mM EDTA 50 mM NaF 10% Glycerol 1% Triton X100 4mM Imidazole 1M 0.6% Lysozyme 1 Protease inhibitor cocktail tablet 1 mM phenylmethylsulphonyl fluoride
4% PFA	**1X PBST**
1X PBST 4% (w/v) Paraformaldehyde	0.2 % (v/v) Tween 20 1X PBS
Blocking buffer	**Fly food recipe**

5% (w/v) non-fat dry milk 0.1% (v/v) Triton X100	20.4 l H_20 1,680 g Maize flour 720 g Yeast 1,800 g Syrup 192 g Potassium sodium tartrate tetrahydrate 36 g Nipagin 120 ml Propionic acid
10X PBS pH 7.4	
10.6 mM KH_2PO_4 1.5 M NaCl 30 mM $Na_2PO_4.7H_20$	
10X SDS running buffer	**10X Transfer buffer**
30 g Tris base 144 g Glycine 10 g SDS dH_2O to 1 L	30 g Tris base 144 g Glycine dH_2O to 1 L
10X TBS pH to 7.6	**1X TBST**
24 g of Tris Base 88 g of NaCl dH_2O to 1 L	100 mL 10X TBS 900 mL dH_2O 0.1% (v/v) Tween 20

541

542 **Primers**

Name	Sequence (5' to 3')	Application
rc2263f	CGCGGATCCATCCGGCGAGAGAGTGTCTTTG	Genomic genomic construct of *α-PheRS*
rc2263r	CGGGGTACCTATGCCTGGCGATAATCGTG	
Tyr412Cys & Phe438Cys-F	TCAAGCCGGCGTACAATCCGTGTACCGAGCCCAG	Construct of *α-PheRS*^{Cys} mutation
Tyr412Cys & Phe438Cys-R	CTCCGGCCGACAGACGCCCGAGTTGCCC	
seq r6	GCTCCCATTCATCAGTTCC	Sequencing
seqA r1	CATTTCCACCGTGAGATCCGTC	Sequencing
seqA r2	AACTCTTGTGGGTGACCGTTTC	Sequencing
seqA f1	GTTCTCGAAGTGAATGTTCTGG	Sequencing
seqA f2	TTTAGCCACCGTCGTCGTTTC	Sequencing
seqA r3	TCCAGCGACGATGACGAATTTG	Sequencing
seqA f3	CAAATGGATTGTGGGACCAGC	Sequencing
seqA r4	GCCCTCCTCCACCATCTTTAG	Sequencing

543

544

545 **Fly genetics and husbandry**

546 All *Drosophila melanogaster* fly stocks were kept for long-term storage at 18ºC in glass or
547 plastic vials on standard food with day/night (12h/12h) light cycles. All experiments were
548 performed at 25ºC unless specifically mentioned. A UAS-GFP element was added in
549 experiments that tested for rescue and involved Gal4-mediated expression of the rescue gene.
550 This construct served to even out the number of UAS sites in each Gal4 expressing cell. Origins
551 of all stocks are noted in the *Key Resource Table*.

552

553 **DNA cloning and generation of transgenic flies**

554 Sequence information was obtained from Flybase. All mutations and the addition of the Myc-
555 tag to the N-terminus of *α-PheRS* were made by following the procedure of the QuickChange
556 Site-Directed Mutagenesis Kit (Stratagene). The genomic *α-PheRS* rescue construct (*Myc::α-*
557 *PheRS*) codes for the entire coding region and an additional Myc tag at the N-terminal end. In
558 addition, it contains ~1kb of up-stream and down-stream sequences and it was cloned into the
559 *pw^{+}SNattB* transformation vector (Koch *et al.*, 2009; Lu *et al.*, 2014). The *α-PheRS* and *β-*
560 *PheRS* cDNAs were obtained by RT-PCR from mRNA isolated from 4-8 days old *OreR* flies
561 (Lu *et al.*, 2014). Transgenic flies were generated by applying the *ϕ* C31-based integration
562 system with the stock (*y w att2A[vas-ϕ]; +; attP-86F*) (Bischof et al., 2007).

563

564 **Western blotting**

565 Protein was extracted from tissues, whole larvae, or flies using lysis buffer. 25 guts were
566 analyzed for each genotype. Protein lysates were separated by SDS-PAGE and transferred onto
567 PVDF membranes (Milipore, US). The blocking was performed for 1h at room temperature

568 (RT) with non-fat dry milk (5%) in TBST solution. Blots were probed first with primary
569 antibodies (diluted in blocking buffer) overnight at 4ºC and then with secondary antibodies
570 (diluted in TBST) 1h at RT. The signal of the secondary antibody was detected by using the
571 detect solution mixture (1:1) (ECL Prime Western Blotting System, GE Healthcare Life
572 Science) and a luminescent detector (Amersham Imager 600, GE Healthcare Life Science).
573 Origins and recipes of all buffers and reagents are noted in the *Key Resource Table*.

574

575 **Immunofluorescent staining and confocal microscopy**

576 Adult midguts were dissected from each female fly after 5 days at 29ºC (unless stated
577 otherwise) or at different time points after 2, 3, 4 days of heat treatment for the time-course
578 experiment. A total of 10 guts were analyzed for each genotype. In the larval experiments, the
579 animals were mated at 25ºC on fresh, rich diet food and set up for egg-laying during a 2-hour
580 window. 120 hours after egg-laying, larval midguts were dissected from wandering third instar
581 larvae and a total of 10 guts were analyzed for each genotype. Dissections were performed in
582 1X PBS on ice and tissues were collected within a maximum of one hour. Fixation with 4%
583 PFA in PBS-T 0.2% at RT was done for different durations depending on the different tissues:
584 two hours (guts), 40 minutes (brains), 30 minutes (wing discs, ovaries). Then the samples were
585 blocked overnight with a blocking buffer at 4ºC. Primary antibodies (diluted in blocking buffer)
586 were incubated with the samples for 8h at RT. The samples were rinsed 3 times and washed 3
587 times (20 minutes/wash) with PBST. Secondary antibodies (diluted in PBST) were incubated
588 overnight at 4ºC. The samples were then rinsed 3 times and washed 2 times (20 minutes/wash)
589 with PBST. Hoechst 33258 (2.5 µg/ml) was added in PBST before the third and last washing
590 step and the samples were mounted with Aqua/Poly Mount solution (Polysciences Inc., US).
591 For the anti-Delta labeling, the samples were blocked for 3h at RT with a blocking buffer. The

592 primary anti-Delta antibody (1:10 v/v) was incubated with the samples overnight at 4ºC and
593 then the secondary antibody was incubated overnight at 4ºC. Origins and diluted concentrations
594 of all buffers and antibodies are noted in the *Key Resource Table*.

595

596 **Image acquisition and processing**

597 Imaging was carried out with a Leica SP8 confocal laser scanning microscope equipped with
598 a 405 nm diode laser, a 458, 476, 488, 496, and 514 nm Argon laser, a 561 nm diode-pumped
599 solid-state laser, and a 633 nm HeNe laser. Images were obtained with 20x dry and 63x oil-
600 immersion objectives and 1024x1024 pixel format. Images were acquired using LAS X
601 software. The images of the entire gut were obtained by imaging at the standard size and then
602 merging maximal projections of Z-stacks with the Tiles Scan tool. Fluorescent intensity was
603 determined from FIJI software.

604

605 **Quantification of cell numbers per posterior midgut**

606 Z stack images through the width of the posterior midgut were acquired along the length of the
607 posterior midgut from the R4a compartment to the midgut-hindgut junction. Maximum
608 projections of each Z stack were obtained, and the total numbers of each cell type were counted
609 manually and exported to Microsoft Excel and GraphPad Prism for further statistical analysis.

610

611 **Quantification and statistical analysis**

612 For quantifications of all experiments, *n* represents the number of independent biological
613 samples analyzed (the number of guts, the number of wing discs, the number of twin spots),
614 error bars represent standard deviation (SD). Statistical significance was determined using the
615 t-test or ANOVA as noted in the figure legends. They were expressed as P values. (*) denotes

616 $p < 0.05$, (**) denotes $p < 0.01$, (***) denotes $p < 0.001$, (****) denotes $p < 0.0001$. (*ns*)
617 denotes values whose difference was not significant.
618
619
620
621

622 Acknowledgments

623 We thank Peter Nagy, Hugo Stocker, Albena Jordanova, Erik Storkebaum, and the
624 Bloomington Stock Center for fly stocks. We are also grateful to Rohan Chippalkatti for
625 sharing his knowledge about the larval brain.
626

627 Financial Disclosure statement

628 This work was supported by a grant from the Novartis Foundation for Medical-Biological
629 Research (#18A050) and by the project grants 31003A_173188 and 310030_205075 from the
630 Swiss National Science Foundation (SNF) to B.S. Equipment support was by an equipment
631 grant from SNF (316030_150824) and by the University of Bern. Additional salary and
632 material support was received from the University of Bern to B.S. The funders had no role in
633 study design, data collection and analysis, decision to publish, or preparation of the manuscript.

634 # References

635 Ables, J.L., Breunig, J.J., Eisch, A.J., and Rakic, P. (2011). Not(ch) just development: Notch
636 signalling in the adult brain. Nature reviews. Neuroscience *12*, 269-283. 10.1038/nrn3024.

637 Barrick, D., and Kopan, R. (2006). The Notch transcription activation complex makes its
638 move. Cell *124*, 883-885. 10.1016/j.cell.2006.02.028.

639 Beehler-Evans, R., and Micchelli, C.A. (2015). Generation of enteroendocrine cell diversity
640 in midgut stem cell lineages. Development *142*, 654-664. 10.1242/dev.114959.

641 Biehs, B., Sturtevant, M.A., and Bier, E. (1998). Boundaries in the Drosophila wing imaginal
642 disc organize vein-specific genetic programs. Development *125*, 4245-4257.

643 Bischof, J., Maeda, R.K., Hediger, M., Karch, F., and Basler, K. (2007). An optimized
644 transgenesis system for Drosophila using germ-line-specific phiC31 integrases. Proceedings
645 of the National Academy of Sciences of the United States of America *104*, 3312-3317.
646 10.1073/pnas.0611511104.

647 Borggrefe, T., and Oswald, F. (2009). The Notch signaling pathway: transcriptional
648 regulation at Notch target genes. Cellular and molecular life sciences : CMLS *66*, 1631-1646.
649 10.1007/s00018-009-8668-7.

650 Borggrefe, T., and Oswald, F. (2016). Setting the Stage for Notch: The Drosophila Su(H)-
651 Hairless Repressor Complex. PLoS biology *14*, e1002524. 10.1371/journal.pbio.1002524.

652 Bray, S., and Furriols, M. (2001). Notch pathway: making sense of suppressor of hairless.
653 Current biology : CB *11*, R217-221. 10.1016/s0960-9822(01)00109-9.

654 Casas-Tinto, S., Lolo, F.N., and Moreno, E. (2015). Active JNK-dependent secretion of
655 Drosophila Tyrosyl-tRNA synthetase by loser cells recruits haemocytes during cell
656 competition. Nature communications *6*, 10022. 10.1038/ncomms10022.

657 Collins, K.J., Yuan, Z., and Kovall, R.A. (2014). Structure and function of the CSL-KyoT2
658 corepressor complex: a negative regulator of Notch signaling. Structure *22*, 70-81.
659 10.1016/j.str.2013.10.010.

660 de Celis, J.F., de Celis, J., Ligoxygakis, P., Preiss, A., Delidakis, C., and Bray, S. (1996).
661 Functional relationships between Notch, Su(H) and the bHLH genes of the E(spl) complex:
662 the E(spl) genes mediate only a subset of Notch activities during imaginal development.
663 Development *122*, 2719-2728.

664 de la Pompa, J.L., Wakeham, A., Correia, K.M., Samper, E., Brown, S., Aguilera, R.J.,
665 Nakano, T., Honjo, T., Mak, T.W., Rossant, J., and Conlon, R.A. (1997). Conservation of the
666 Notch signalling pathway in mammalian neurogenesis. Development *124*, 1139-1148.

667 Deng, W.M., Althauser, C., and Ruohola-Baker, H. (2001). Notch-Delta signaling induces a
668 transition from mitotic cell cycle to endocycle in Drosophila follicle cells. Development *128*,
669 4737-4746.

670 Finarov, I., Moor, N., Kessler, N., Klipcan, L., and Safro, M.G. (2010). Structure of human
671 cytosolic phenylalanyl-tRNA synthetase: evidence for kingdom-specific design of the active
672 sites and tRNA binding patterns. Structure *18*, 343-353. 10.1016/j.str.2010.01.002.

673 Fortini, M.E., and Artavanis-Tsakonas, S. (1994). The suppressor of hairless protein
674 participates in notch receptor signaling. Cell *79*, 273-282. 10.1016/0092-8674(94)90196-1.

675 Furriols, M., and Bray, S. (2001). A model Notch response element detects Suppressor of
676 Hairless-dependent molecular switch. Current biology : CB *11*, 60-64. 10.1016/s0960-
677 9822(00)00044-0.

678 Giachino, C., and Taylor, V. (2014). Notching up neural stem cell homogeneity in
679 homeostasis and disease. Frontiers in neuroscience *8*, 32. 10.3389/fnins.2014.00032.

680 Gomard-Mennesson, E., Fabien, N., Cordier, J.F., Ninet, J., Tebib, J., and Rousset, H. (2007).
681 Clinical significance of anti-histidyl-tRNA synthetase (Jo1) autoantibodies. Annals of the
682 New York Academy of Sciences *1109*, 414-420. 10.1196/annals.1398.047.

683 Gordon, W.R., Arnett, K.L., and Blacklow, S.C. (2008). The molecular logic of Notch
684 signaling--a structural and biochemical perspective. Journal of cell science *121*, 3109-3119.
685 10.1242/jcs.035683.

686 Grandbarbe, L., Bouissac, J., Rand, M., Hrabe de Angelis, M., Artavanis-Tsakonas, S., and
687 Mohier, E. (2003). Delta-Notch signaling controls the generation of neurons/glia from neural
688 stem cells in a stepwise process. Development *130*, 1391-1402.

689 Greenberg, Y., King, M., Kiosses, W.B., Ewalt, K., Yang, X., Schimmel, P., Reader, J.S., and
690 Tzima, E. (2008). The novel fragment of tyrosyl tRNA synthetase, mini-TyrRS, is secreted to
691 induce an angiogenic response in endothelial cells. FASEB journal : official publication of
692 the Federation of American Societies for Experimental Biology *22*, 1597-1605.
693 10.1096/fj.07-9973com.

694 Guo, M., and Schimmel, P. (2013). Essential nontranslational functions of tRNA synthetases.
695 Nature chemical biology *9*, 145-153. 10.1038/nchembio.1158.

696 Guo, Z., Lucchetta, E., Rafel, N., and Ohlstein, B. (2016). Maintenance of the adult
697 Drosophila intestine: all roads lead to homeostasis. Current opinion in genetics &
698 development *40*, 81-86. 10.1016/j.gde.2016.06.009.

699 Guo, Z., and Ohlstein, B. (2015). Stem cell regulation. Bidirectional Notch signaling
700 regulates Drosophila intestinal stem cell multipotency. Science *350*.
701 10.1126/science.aab0988.

Hatakeyama, J., Bessho, Y., Katoh, K., Ookawara, S., Fujioka, M., Guillemot, F., and Kageyama, R. (2004). Hes genes regulate size, shape and histogenesis of the nervous system by control of the timing of neural stem cell differentiation. Development *131*, 5539-5550. 10.1242/dev.01436.

Henrique, D., and Schweisguth, F. (2019). Mechanisms of Notch signaling: a simple logic deployed in time and space. Development *146*. 10.1242/dev.172148.

Ho, M.T., Lu, J., Dominique Brunßen and Suter, B. (2021). A translation-independent function of PheRS activates growth and proliferation in Drosophila. Disease Models & Mechanisms 14, dmm048132. doi:10.1242/dmm.048132.

Hori, K., Sen, A., and Artavanis-Tsakonas, S. (2013). Notch signaling at a glance. Journal of cell science *126*, 2135-2140. 10.1242/jcs.127308.

Houtz, P., Bonfini, A., Bing, X., and Buchon, N. (2019). Recruitment of Adult Precursor Cells Underlies Limited Repair of the Infected Larval Midgut in Drosophila. Cell host & microbe *26*, 412-425 e415. 10.1016/j.chom.2019.08.006.

Jiang, H., and Edgar, B.A. (2011). Intestinal stem cells in the adult Drosophila midgut. Experimental cell research *317*, 2780-2788. 10.1016/j.yexcr.2011.07.020.

Johannes, B., and Preiss, A. (2002). Wing vein formation in Drosophila melanogaster: hairless is involved in the cross-talk between Notch and EGF signaling pathways. Mechanisms of development *115*, 3-14. 10.1016/s0925-4773(02)00083-7.

Johnson, S.E., Ilagan, M.X., Kopan, R., and Barrick, D. (2010). Thermodynamic analysis of the CSL x Notch interaction: distribution of binding energy of the Notch RAM region to the CSL beta-trefoil domain and the mode of competition with the viral transactivator EBNA2. J Biol Chem *285*, 6681-6692. 10.1074/jbc.M109.019968.

Koch, R., Ledermann, R., Urwyler, O., Heller, M., and Suter, B. (2009). Systematic functional analysis of Bicaudal-D serine phosphorylation and intragenic suppression of a female sterile allele of BicD. PloS one *4*, e4552. 10.1371/journal.pone.0004552.

Korzelius, J., Azami, S., Ronnen-Oron, T., Koch, P., Baldauf, M., Meier, E., Rodriguez-Fernandez, I.A., Groth, M., Sousa-Victor, P., and Jasper, H. (2019). The WT1-like transcription factor Klumpfuss maintains lineage commitment of enterocyte progenitors in the Drosophila intestine. Nat Commun *10*, 4123. 10.1038/s41467-019-12003-0.

Korzelius, J., Naumann, S.K., Loza-Coll, M.A., Chan, J.S., Dutta, D., Oberheim, J., Glasser, C., Southall, T.D., Brand, A.H., Jones, D.L., and Edgar, B.A. (2014). Escargot maintains stemness and suppresses differentiation in Drosophila intestinal stem cells. EMBO J *33*, 2967-2982. 10.15252/embj.201489072.

736 Kovall, R.A. (2007). Structures of CSL, Notch and Mastermind proteins: piecing together an
737 active transcription complex. Current opinion in structural biology *17*, 117-127.
738 10.1016/j.sbi.2006.11.004.

739 Lee, J.H., and Lee, W.J. (2019). Stealing from the Future: Injured Larvae Spend Stem Cell
740 Deposits. Cell host & microbe *26*, 301-303. 10.1016/j.chom.2019.08.013.

741 Lee, S.W., Cho, B.H., Park, S.G., and Kim, S. (2004). Aminoacyl-tRNA synthetase
742 complexes: beyond translation. Journal of cell science *117*, 3725-3734. 10.1242/jcs.01342.

743 Lian, T., Wu, Q., Hodge, B.A., Wilson, K.A., Yu, G., and Yang, M. (2018). Drosophila Gut-
744 A Nexus Between Dietary Restriction and Lifespan. International journal of molecular
745 sciences *19*. 10.3390/ijms19123810.

746 Ling, J., Yadavalli, S.S., and Ibba, M. (2007). Phenylalanyl-tRNA synthetase editing defects
747 result in efficient mistranslation of phenylalanine codons as tyrosine. RNA *13*, 1881-1886.
748 10.1261/rna.684107.

749 Liu, J., Sato, C., Cerletti, M., and Wagers, A. (2010). Notch signaling in the regulation of
750 stem cell self-renewal and differentiation. Current topics in developmental biology *92*, 367-
751 409. 10.1016/S0070-2153(10)92012-7.

752 Lopez-Schier, H., and St Johnston, D. (2001). Delta signaling from the germ line controls the
753 proliferation and differentiation of the somatic follicle cells during Drosophila oogenesis.
754 Genes & development *15*, 1393-1405. 10.1101/gad.200901.

755 Loza-Coll, M.A., Southall, T.D., Sandall, S.L., Brand, A.H., and Jones, D.L. (2014).
756 Regulation of Drosophila intestinal stem cell maintenance and differentiation by the
757 transcription factor Escargot. The EMBO journal *33*, 2983-2996. 10.15252/embj.201489050.

758 Lu, J., Bergert, M., Walther, A., and Suter, B. (2014). Double-sieving-defective aminoacyl-
759 tRNA synthetase causes protein mistranslation and affects cellular physiology and
760 development. Nature communications *5*, 5650. 10.1038/ncomms6650.

761 Maier, D. (2019). The evolution of transcriptional repressors in the Notch signaling pathway:
762 a computational analysis. Hereditas *156*, 5. 10.1186/s41065-019-0081-0.

763 Marianes, A., and Spradling, A.C. (2013). Physiological and stem cell compartmentalization
764 within the Drosophila midgut. eLife *2*, e00886. 10.7554/eLife.00886.

765 Mathur, D., Bost, A., Driver, I., and Ohlstein, B. (2010). A transient niche regulates the
766 specification of Drosophila intestinal stem cells. Science *327*, 210-213.
767 10.1126/science.1181958.

768 Micchelli, C.A. (2012). The origin of intestinal stem cells in Drosophila. Developmental
769 dynamics *241*, 85-91. 10.1002/dvdy.22759.

770 Micchelli, C.A., and Perrimon, N. (2006). Evidence that stem cells reside in the adult
771 Drosophila midgut epithelium. Nature *439*, 475-479. 10.1038/nature04371.

772 Mundorf, J., Donohoe, C.D., McClure, C.D., Southall, T.D., and Uhlirova, M. (2019). Ets21c
773 Governs Tissue Renewal, Stress Tolerance, and Aging in the Drosophila Intestine. Cell
774 reports *27*, 3019-3033 e3015. 10.1016/j.celrep.2019.05.025.

775 Nagel, A.C., Auer, J.S., Schulz, A., Pfannstiel, J., Yuan, Z., Collins, C.E., Kovall, R.A., and
776 Preiss, A. (2017). Phosphorylation of Suppressor of Hairless impedes its DNA-binding
777 activity. Scientific reports *7*, 11820. 10.1038/s41598-017-11952-0.

778 Nagy, P., Sandor, G.O., and Juhasz, G. (2018). Autophagy maintains stem cells and intestinal
779 homeostasis in Drosophila. Scientific reports *8*, 4644. 10.1038/s41598-018-23065-3.

780 Nathanson, L., and Deutscher, M.P. (2000). Active aminoacyl-tRNA synthetases are present
781 in nuclei as a high molecular weight multienzyme complex. The Journal of biological
782 chemistry *275*, 31559-31562. 10.1074/jbc.C000385200.

783 Ohlstein, B., and Spradling, A. (2006). The adult Drosophila posterior midgut is maintained
784 by pluripotent stem cells. Nature *439*, 470-474. 10.1038/nature04333.

785 Ohlstein, B., and Spradling, A. (2007). Multipotent Drosophila intestinal stem cells specify
786 daughter cell fates by differential notch signaling. Science *315*, 988-992.
787 10.1126/science.1136606.

788 Oswald, F., and Kovall, R.A. (2018). CSL-Associated Corepressor and Coactivator
789 Complexes. Adv Exp Med Biol *1066*, 279-295. 10.1007/978-3-319-89512-3_14.

790 Otani, A., Slike, B.M., Dorrell, M.I., Hood, J., Kinder, K., Ewalt, K.L., Cheresh, D.,
791 Schimmel, P., and Friedlander, M. (2002). A fragment of human TrpRS as a potent
792 antagonist of ocular angiogenesis. Proceedings of the National Academy of Sciences of the
793 United States of America *99*, 178-183. 10.1073/pnas.012601899.

794 Park, S.J., Yoon, B.H., Kim, S.K., and Kim, S.Y. (2019). GENT2: an updated gene
795 expression database for normal and tumor tissues. BMC medical genomics *12*, 101.
796 10.1186/s12920-019-0514-7.

797 Praxenthaler, H., Nagel, A.C., Schulz, A., Zimmermann, M., Meier, M., Schmid, H., Preiss,
798 A., and Maier, D. (2017). Hairless-binding deficient Suppressor of Hairless alleles reveal
799 Su(H) protein levels are dependent on complex formation with Hairless. PLoS genetics *13*,
800 e1006774. 10.1371/journal.pgen.1006774.

801 Qiao, L., and Wong, B.C. (2009). Role of Notch signaling in colorectal cancer.
802 Carcinogenesis *30*, 1979-1986. 10.1093/carcin/bgp236.

803 Rodova, M., Ankilova, V., and Safro, M.G. (1999). Human phenylalanyl-tRNA synthetase:
804 cloning, characterization of the deduced amino acid sequences in terms of the structural
805 domains and coordinately regulated expression of the alpha and beta subunits in chronic
806 myeloid leukemia cells. Biochemical and biophysical research communications *255*, 765-
807 773. 10.1006/bbrc.1999.0141.

808 Roy, H., and Ibba, M. (2006). Phenylalanyl-tRNA synthetase contains a dispensable RNA-
809 binding domain that contributes to the editing of noncognate aminoacyl-tRNA. Biochemistry
810 *45*, 9156-9162. 10.1021/bi060549w.

811 Saj, A., Arziman, Z., Stempfle, D., van Belle, W., Sauder, U., Horn, T., Durrenberger, M.,
812 Paro, R., Boutros, M., and Merdes, G. (2010). A combined ex vivo and in vivo RNAi screen
813 for notch regulators in Drosophila reveals an extensive notch interaction network.
814 Developmental cell *18*, 862-876. 10.1016/j.devcel.2010.03.013.

815 Schimmel, P.R., and Soll, D. (1979). Aminoacyl-tRNA synthetases: general features and
816 recognition of transfer RNAs. Annual review of biochemistry *48*, 601-648.
817 10.1146/annurev.bi.48.070179.003125.

818 Sen, S., Zhou, H., Ripmaster, T., Hittelman, W.N., Schimmel, P., and White, R.A. (1997).
819 Expression of a gene encoding a tRNA synthetase-like protein is enhanced in tumorigenic
820 human myeloid leukemia cells and is cell cycle stage- and differentiation-dependent.
821 Proceedings of the National Academy of Sciences of the United States of America *94*, 6164-
822 6169.

823 Shcherbata, H.R., Althauser, C., Findley, S.D., and Ruohola-Baker, H. (2004). The mitotic-
824 to-endocycle switch in Drosophila follicle cells is executed by Notch-dependent regulation of
825 G1/S, G2/M and M/G1 cell-cycle transitions. Development *131*, 3169-3181.
826 10.1242/dev.01172.

827 Shimmi, O., Matsuda, S., and Hatakeyama, M. (2014). Insights into the molecular
828 mechanisms underlying diversified wing venation among insects. Proceedings. Biological
829 sciences *281*, 20140264. 10.1098/rspb.2014.0264.

830 Smirnova, E.V., Lakunina, V.A., Tarassov, I., Krasheninnikov, I.A., and Kamenski, P.A.
831 (2012). Noncanonical functions of aminoacyl-tRNA synthetases. Biochemistry. Biokhimiia
832 *77*, 15-25. 10.1134/S0006297912010026.

833 Tabaja, N., Yuan, Z., Oswald, F., and Kovall, R.A. (2017). Structure-function analysis of
834 RBP-J-interacting and tubulin-associated (RITA) reveals regions critical for repression of
835 Notch target genes. J Biol Chem *292*, 10549-10563. 10.1074/jbc.M117.791707.

836 Taniguchi, Y., Furukawa, T., Tun, T., Han, H., and Honjo, T. (1998). LIM protein KyoT2
837 negatively regulates transcription by association with the RBP-J DNA-binding protein. Mol
838 Cell Biol *18*, 644-654. 10.1128/MCB.18.1.644.

839 Teleman, A.A., and Cohen, S.M. (2000). Dpp gradient formation in the Drosophila wing
840 imaginal disc. Cell *103*, 971-980. 10.1016/s0092-8674(00)00199-9.

841 Thurmond, J., Goodman, J.L., Strelets, V.B., Attrill, H., Gramates, L.S., Marygold, S.J.,
842 Matthews, B.B., Millburn, G., Antonazzo, G., Trovisco, V., et al. (2019). FlyBase 2.0: the
843 next generation. Nucleic acids research *47*, D759-D765. 10.1093/nar/gky1003.

844 Wacker, S.A., Alvarado, C., von Wichert, G., Knippschild, U., Wiedenmann, J., Clauss, K.,
845 Nienhaus, G.U., Hameister, H., Baumann, B., Borggrefe, T., et al. (2011). RITA, a novel
846 modulator of Notch signalling, acts via nuclear export of RBP-J. EMBO J *30*, 43-56.
847 10.1038/emboj.2010.289.

848 Yin, L., Velazquez, O.C., and Liu, Z.J. (2010). Notch signaling: emerging molecular targets
849 for cancer therapy. Biochemical pharmacology *80*, 690-701. 10.1016/j.bcp.2010.03.026.

850 Zeng, X., and Hou, S.X. (2015). Enteroendocrine cells are generated from stem cells through
851 a distinct progenitor in the adult Drosophila posterior midgut. Development *142*, 644-653.
852 10.1242/dev.113357.

853 Zhai, Z., Boquete, J.P., and Lemaitre, B. (2017). A genetic framework controlling the
854 differentiation of intestinal stem cells during regeneration in Drosophila. PLoS genetics *13*,
855 e1006854. 10.1371/journal.pgen.1006854.

856 Zhai, Z., Kondo, S., Ha, N., Boquete, J.P., Brunner, M., Ueda, R., and Lemaitre, B. (2015).
857 Accumulation of differentiating intestinal stem cell progenies drives tumorigenesis. Nature
858 communications *6*, 10219. 10.1038/ncomms10219.

859 Zhou, J.J., Wang, F., Xu, Z., Lo, W.S., Lau, C.F., Chiang, K.P., Nangle, L.A., Ashlock,
860 M.A., Mendlein, J.D., Yang, X.L., et al. (2014). Secreted histidyl-tRNA synthetase splice
861 variants elaborate major epitopes for autoantibodies in inflammatory myositis. The Journal of
862 biological chemistry *289*, 19269-19275. 10.1074/jbc.C114.571026.

863 Zimber-Strobl, U., and Strobl, L.J. (2001). EBNA2 and Notch signalling in Epstein-Barr
864 virus mediated immortalization of B lymphocytes. Semin Cancer Biol *11*, 423-434.
865 10.1006/scbi.2001.0409.

866

867

868 **Figure legends:**

869

870 **Figure 1: α-PheRS is enriched in *Drosophila* progenitor and enteroendocrine cells.**

871 (A-A", B, C-C", D) Endogenous α-PheRS accumulation is higher in small, diploid progenitor
872 cells in wild-type adult and larval midguts. Signal intensity values in the graphs (right column)
873 were measured from left to right along the lines in B and D. (E-F"") The *esg-Gal4,UAS-*
874 *2XEYFP;tub-Gal80^{ts}* (=esg^{ts}) system and Prospero staining, respectively, were used to label
875 progenitor and enteroendocrine cells, respectively. Animals were mated at 18°C and adults of
876 the required genotypes were collected and shifted to 29°C to inactivate Gal80^{ts}. Adult midguts
877 were dissected from female flies after 5 days of induction.

878

879

880 **Figure 2: Elevated α-PheRS levels affect gut homeostasis, leading to additional progenitor**
881 **cells, EEs, and differentiating EBs.**

882 (A-C"') Elevated α-PheRS or α-PheRS^{Cys} levels induced by the esg^{ts} system (see Fig 1E for
883 details) led to additional YFP-positive cells and also to the accumulation of EEs *(*esg^{ts}*/+;UAS-*
884 *α-PheRS$^{(Cys)}$/+)*. (D-D"') RNAi knockdown of *Notch (N)* with the same esg^{ts} system led to a
885 similar phenotype as elevation of α-PheRS levels *(UAS-N^{RNAi}/+;* esg^{ts}*/+)*. (E-F"') Elevation of
886 α-PheRS levels rescued the depleted ISC pool caused by Notch over-activation (induced by
887 expressing the NICD under esg^{ts} control). (G) Quantification of YFP^{+} cell numbers. (H)
888 Proportional contribution of EEs to the total number of gut cells in the intestinal region
889 analyzed. (I) Percentage of differentiating EBs among YFP^{+} cells. In all experiments, EEs were
890 visualized with the anti-Prospero antibody, YFP^{-}/Hoechst^{+} polyploid cells were counted as
891 ECs. Animals were mated at 18°C, and adults of the required genotypes were collected and
892 shifted to 29°C to inactivate Gal80^{ts}. Adult midguts were dissected from female flies after 5
893 days of induction at 29°C. At least 10 guts were analyzed for each genotype. n=10, **p<0.01,
894 ***p<0.001, ****p<0.0001 in ANOVA tests. (J) The Notch activity reporter (NRE-eGFP)
895 expresses GFP under the control of a Notch response element. Its levels drastically decreased
896 upon elevated expression of *α-PheRS* or *α-PheRS^{Cys}* in adult midgut ISCs (*esg-Gal4,UAS-*
897 *2XEYFP/+;tub-Gal80^{ts}/UAS-α-PheRS$^{(Cys)}$,NRE-eGFP)*. Female flies were collected 3 days
898 after eclosure and cultured at 29°C for 5 days before dissecting and harvesting their midguts.

899

900

901 **Figure 3: The phenotype of elevated α-PheRS levels resembles partially a *Notch*-like**
902 **phenotype in larval guts.**

903 (A-H) Whole gut images and high-power micrographs of the posterior midgut area marked
904 with a white square in the overview picture. The expression of the different genes indicated
905 was driven with the *esg-Gal4,UAS-2XEYFP* system. The YFP signal displayed in green marks
906 AMPs and EBs, Hoechst (blue) marks the nuclear DNA. (C) Elevated *α-PheRS^{Cys}* expression
907 gave rise to tumor-like areas in both the anterior and the posterior midgut (outlined with dashed

908 lines) (*esg-Gal4,UAS-2XEYFP/+;UAS-α-PheRS$^{(Cys)}$/+)*. (E-E", F) Mitotic cells were identified
909 with anti-phospho-Histone H3 (PH3) antibodies (red channel) and the PH3+ cells are counted
910 and normalized to the total cell number per intestinal region. n=10, **p<0.01, ***p<0.001 in
911 t-tests. (G) Total cells per intestinal region (total cells per frame of 63x objective of confocal
912 microscope with 1024x1024 pixels) were measured by counting Hoechst 33258 labeled cells
913 manually. n=10, **p<0.01,****p<0.0001.

914

915

916 **Figure 4: *α-PheRS* counteracts *Notch* activity in neuroblast proliferation.**

917 (A-F) Additional expression of *α-PheRS* or *α-PheRS^{Cys}* in neuroblasts reduced the ratio of
918 central brain (CB) size to optic lobe (OL) size. The *insc-Gal4,UAS-GFP* system was used to
919 drive the expression of the test genes in neuroblasts (NBs) (*w*, Insc-Gal4/UAS-GFP;UAS-α-*
920 *PheRS$^{(Cys)}$/+)*. NBs were labeled by GFP expression. CBs are shown on the right side (area
921 with GFP^{+} NBs and outlined by white dashed lines) and the OL area on the left. (G) Effect of
922 increased expression of *α-PheRS$^{(Cys)}$*and *NICD,* and of *N* knockdown on the CB/OL size ratio.
923 n=20, ***p<0.001, *ns*: not significant. (H-M, N) Elevated α-PheRS or α-PheRS^{Cys} levels
924 reduced the number of Type II NBs per brain lobe, and less than half of the lobes contained the
925 normal 7-8 NBs. *Notch* RNAi caused the same phenotype with higher expressivity. Additional
926 expression of *α-PheRS$^{(Cys)}$* rescued the tumor phenotype caused by ectopic Notch activation in
927 NB to normal wild-type levels. The larval brains were dissected from third instar larvae, and
928 at least 20 brains were analyzed for each genotype (*w*,UAS-Dicer2/+;wor-Gal4,ase-*
929 *Gal80/+;UAS-mCD8::GFP/UAS-α-PheRS$^{(Cys)}$).* Each brain lobe was classified according to
930 the number of Type II NBs per brain lobe. n = 25.

931

932

933 **Figure 5: Elevated α-PheRS levels repress Notch signaling in wing discs.**

934 Schematic illustration of wild-type wing imaginal discs showing the position of the different
935 compartments (A), the expression domain of en^{ts}>mRFP (A'), and the expression domain of
936 *NRE-eGFP* (A") along the dorsal/ventral (D/V) boundary. (A"') *en-Gal4,NRE-eGFP,UAS-*
937 *mRFP;tub-Gal80^{ts}* was used to drive transgene expression in the posterior compartment of
938 developing wing discs and to evaluate the Notch activity with the reporter *NRE-eGFP* (black
939 arrowhead) *(w,UAS-Dcr2/+;en-Gal4,UAS-mRFP,NRE-eGFP/+;tub-Gal80^{ts}/UAS-α-*
940 *PheRS$^{(Cys)}$).* (B-E"') Elevated α-PheRS or α-PheRS^{Cys} led to the loss of NRE-eGFP expression
941 in the posterior compartment, similar to the phenotype of *Notch* knockdown *(w,UAS-*
942 *Dcr2/UAS-N^{RNAi};en-Gal4,UAS-mRFP,NRE-eGFP/+;tub-Gal80^{ts}/+)*. After egg-laying and
943 incubation at 18°C for 6 days, the animals were shifted to 29°C for 1 day to inactivate Gal80^{ts}
944 and to enable expression of α-PheRS, α-PheRS^{Cys}, or *N^{RNAi}*.

945

946

Figure 6: The N-term of α-PheRS (α-S) is sufficient to induce the proliferative phenotype and repress Notch activity.

(A) 3D model of the α-PheRS structure (suggested by SWISS MODEL tool https://swissmodel.expasy.org/) also shows that the catalytic module and the winged DBDs are separated from each other by a linker strand. (B) Schematic illustration of the α-PheRS polypeptide with its ATP and phenylalanine binding residues. α-PheRS has the catalytic domains located in the C-terminal part and the DNA binding domains (DBD-1,2,3) located in the N-terminal region. The Myc tagged α-S construct lacks all core domains of α-PheRS but encodes the first 200 codons of the α-PheRS ORF under UAS control. (C,D) *Myc::α-S* was expressed using the esg^{ts} system in adult and larval midguts and this led to similar phenotypes as elevated expression of α-PheRS$^{(Cys)}$ in the same system *(*esg^{ts}*/UAS-Myc::α-S)*. (E-E',F,G) Quantification of PH3^{+} cell numbers (F) and the proportion of EE per total cell number (G) in the intestinal region analyzed. In all experiments, EEs were visualized with the anti-Prospero antibody, YFP^{-}/Hoechst^{+} polyploid cells were counted as ECs. Animals were mated at 18ºC, and adults of the required genotypes were collected and shifted to 29ºC to inactivate Gal80^{ts}. Adult midguts were dissected from female flies after 5 days of induction at 29ºC. At least 10 guts were analyzed for each genotype. n=10, **p<0.01, ***p<0.001, ****p<0.0001 in ANOVA tests. (H, H') The ectopic wing venation phenotype resulting from elevated levels of Myc::α-S was similar to the phenotype of elevated α-PheRS$^{(Cys)}$ (shown in Fig 5A). An ectopic vein branches from the connecting vein between the L4 and L5 veins (arrowhead). The same system and experimental settings were used as in Fig 5A *(*en^{ts}*/+;UAS-Myc::α-S/+)*. (I-J') Elevated Myc::α-S leads to the loss of NRE-eGFP expression in the posterior compartments, similar to the effect of α-PheRS$^{(Cys)}$. The same system and experimental setups were used as in Fig 5B-F *(w,UAS-Dcr2/+;en-Gal4,UAS-mRFP,NRE-eGFP/+;tub-Gal80^{ts}/UAS-Myc::α-S)*. (K, L) Besides the full-length α-PheRS isoform (55kDa), one stable Myc-tag containing isoform around 40 KDa and another around 25KDa appear when expressing transgenic Myc::α-PheRS under the control of the *Tub-Gal4* driver *(w; +/+; Tub-Gal4/UAS-Myc::α-PheRS)*. The 40 KDa isoform was present in larval heads and fat bodies, while the 25 KDa isoform was predominantly expressed in larval guts.

977 **Figure 7: Possible mechanism of the competition between N^{ICD} and the α-S activity.**

978 (A) The alignment of Notch and α-PheRS shows that moderately conserved motives are
979 present in the RAM domain (1766-1896 aa) and the N-terminal sequence of α-PheRS (1-180
980 aa). The DNA binding domain (DBD) is shown shaded in green. The alignment task was
981 conducted by the Alignment Tool of the Uniprot website (https://www.uniprot.org/) with two
982 FASTA polypeptide sequences of *Drosophila* Notch and *Drosophila* α-PheRS. * (asterisk)
983 indicates positions that have a single, fully conserved residue. ":" (colon) indicates
984 conservation between groups of strongly similar properties - scoring > 0.5 in the Gonnet PAM
985 250 matrix. A "." (period) indicates conservation between groups of weakly similar properties
986 - scoring =< 0.5 in the Gonnet PAM 250 matrix. (B-D"') Elevated YFP (control), Myc::α-
987 S^{W112A} or α-$PheRS^{W112A}$ levels induced by the esg^{ts} system (see Fig 1E for details) did not lead
988 to additional YFP-positive cells and also not to the hyper-accumulation of EEs. (E- F"') Neither
989 elevated Myc::α-S^{W112A} nor α-$PheRS^{W112A}$ levels rescued the depleted ISC pool caused by
990 Notch over-activation (induced by expressing the NICD under the same control). Note that F
991 shows only 2 $Pros^{+}$ cells, the weaker signals are caused by autofluorescence from some fibers.
992 (G) Quantification of YFP^{+} cell numbers and (H) Proportional contribution of EEs to the total
993 number of gut cells in the intestinal region analyzed (visualized with the 63x objective and
994 Leica SP8). Animals were mated at 18°C, and adults of the required genotypes were collected
995 and shifted to 29°C to inactivate $Gal80^{ts}$. Adult midguts were dissected from female flies after
996 5 days of induction at 29°C. At least 10 guts were analyzed for each genotype. n=10, **p<0.01,
997 ***p<0.001, ****p<0.0001 in ANOVA tests. (I-J"') The anti Myc staining revealed the
998 presence of both Myc::α-S and Myc::α-S^{W112A} in nuclei. Signal intensity values in the graphs
999 (L) and (K) were measured from left to right along the lines in I"' and J"', respectively.

1000

1001

1002

Figure 1

Adult midgut

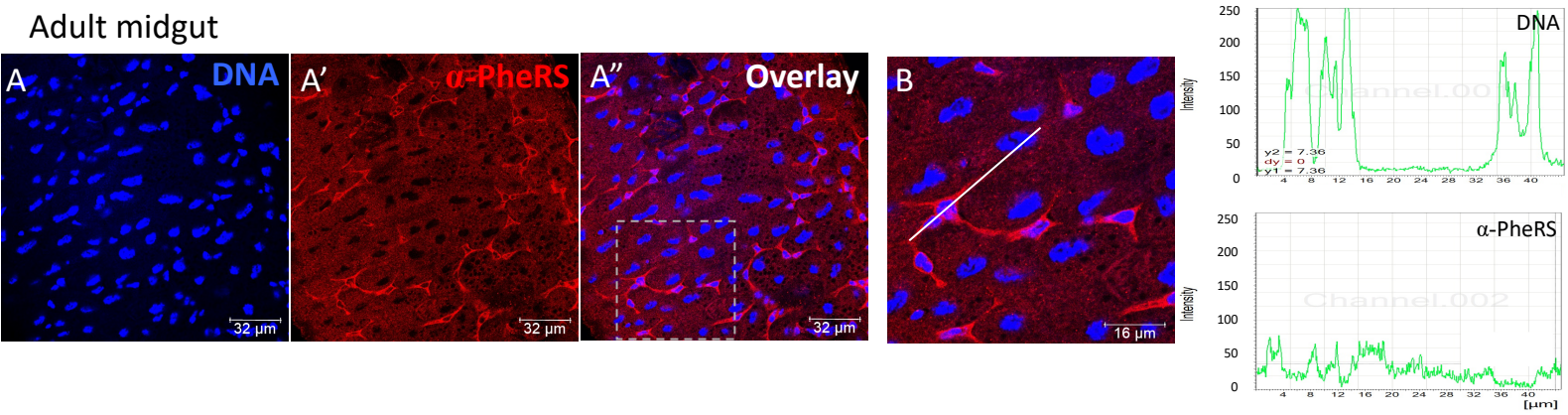

Larval midgut

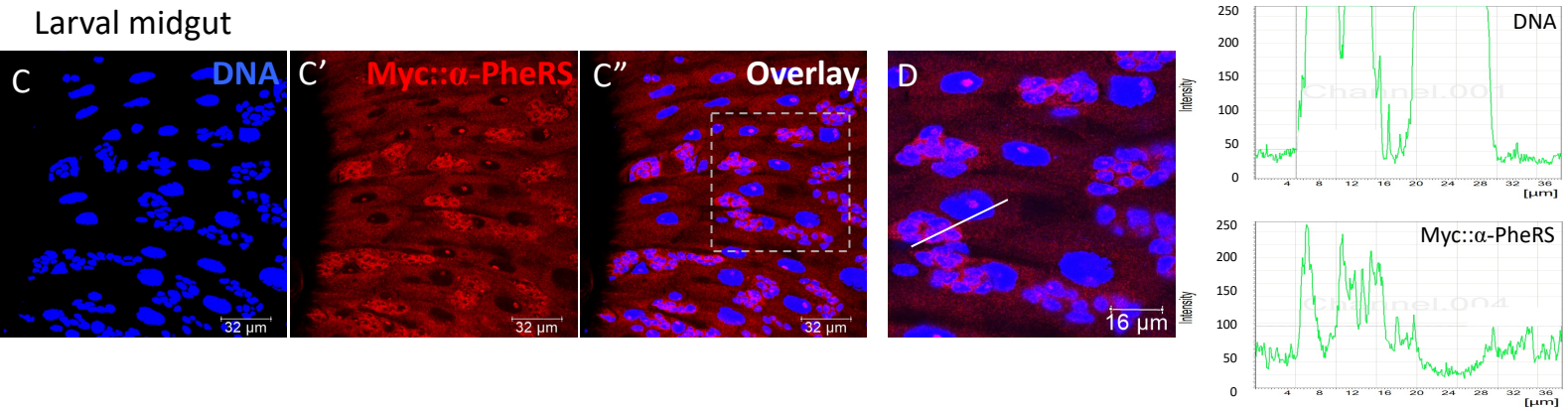

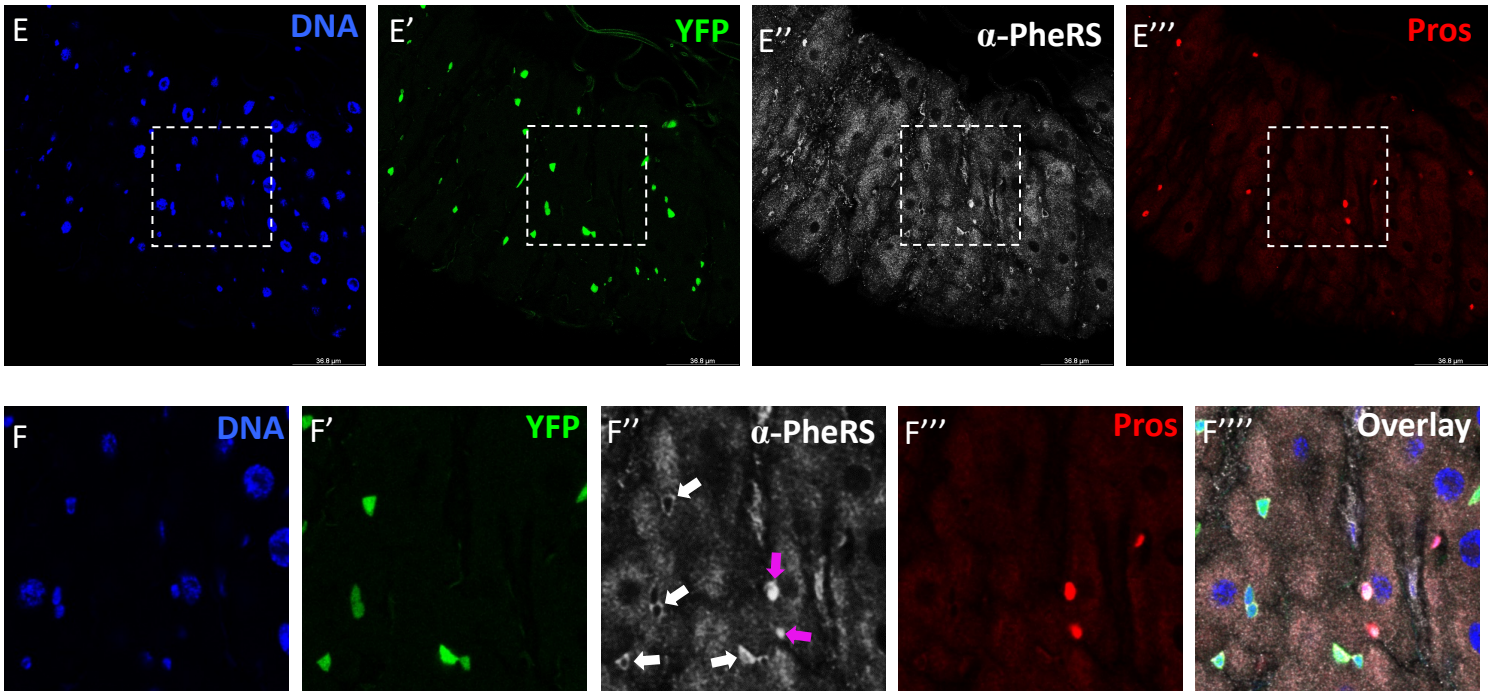

Figure 2

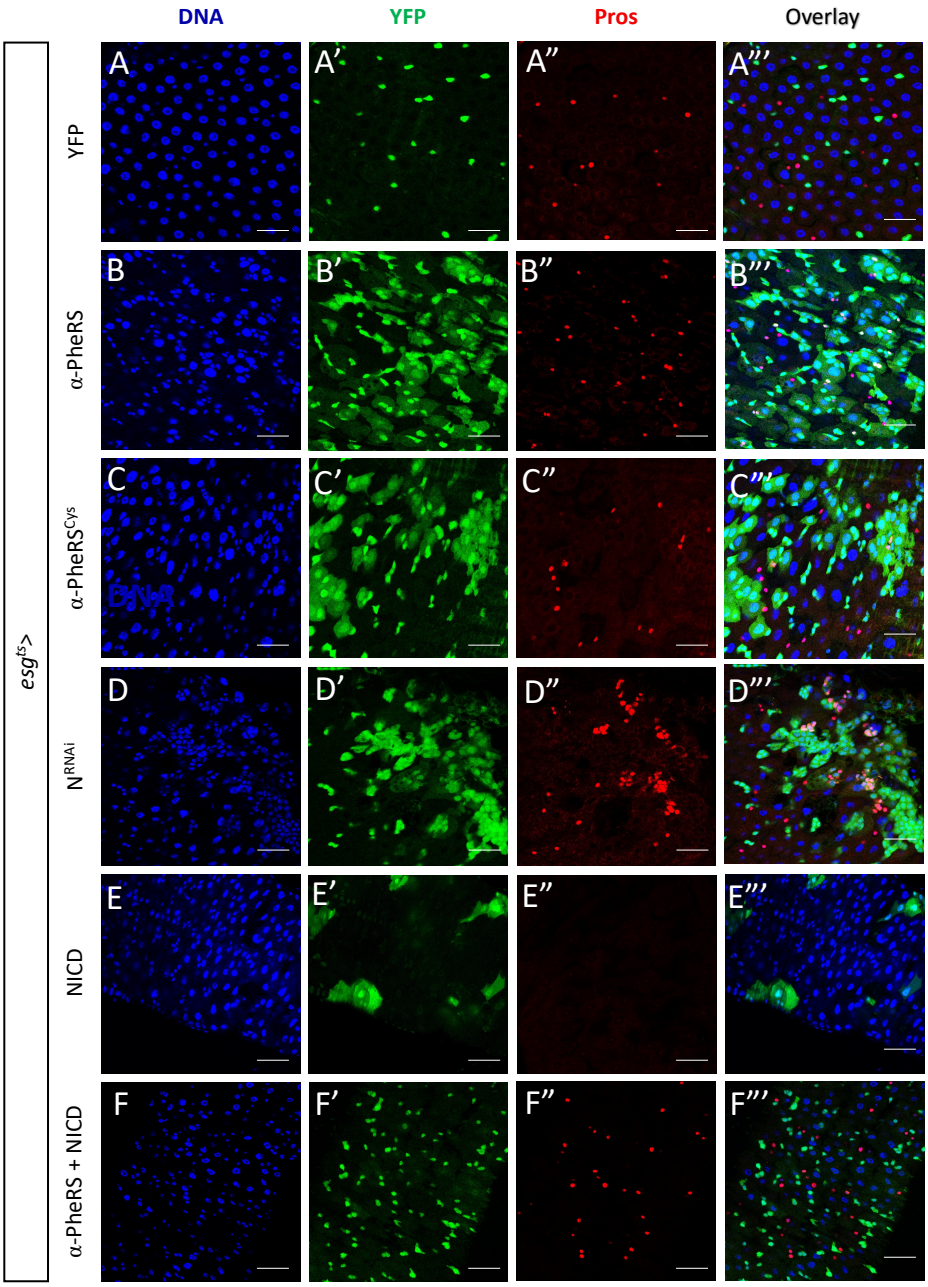
DNA
YFP
Pros
Overlay
esg^ts>
YFP
α-PheRS
α-PheRS^Cys
N^RNAi
NICD
α-PheRS + NICD
A
A'
A''
A'''
B
B'
B''
B'''
C
C'
C''
C'''
D
D'
D''
D'''
E
E'
E''
E'''
F
F'
F''
F'''

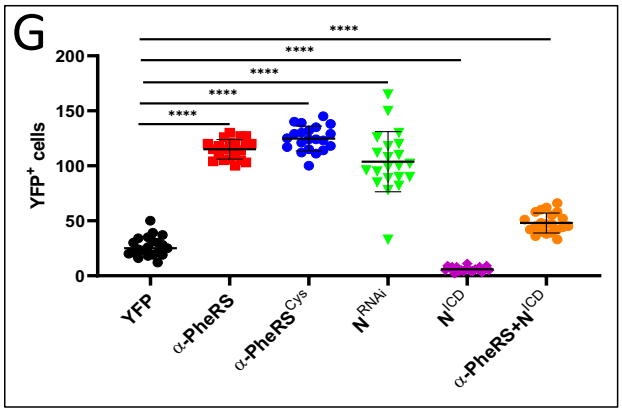
G
YFP+ cells
200
150
100
50
0
****
YFP
α-PheRS
α-PheRS^Cys
N^RNAi
N^ICD
α-PheRS+N^ICD

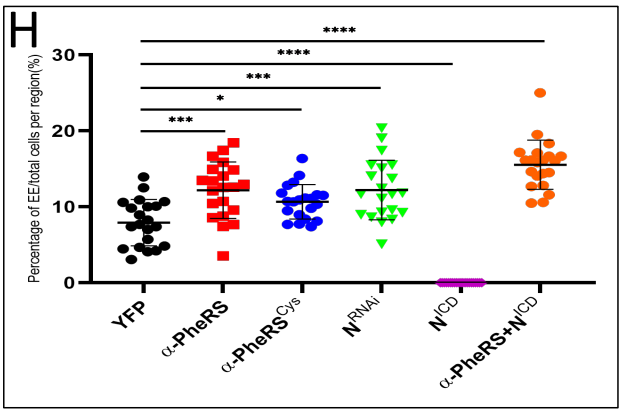
H
Percentage of EE/total cells per region(%)
30
20
10
0
****
***
*
YFP
α-PheRS
α-PheRS^Cys
N^RNAi
N^ICD
α-PheRS+N^ICD

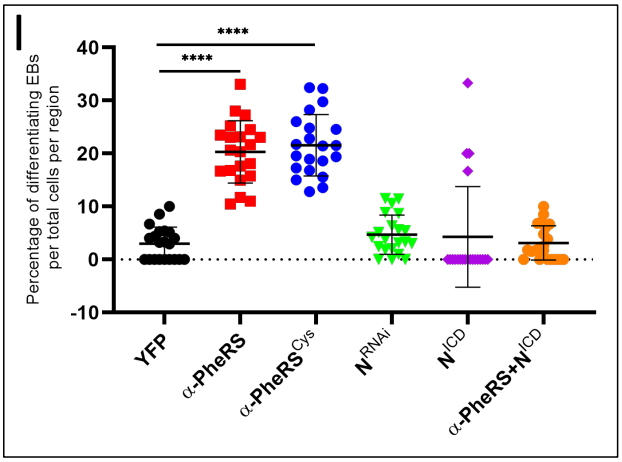
I
Percentage of differentiating EBs per total cells per region
40
30
20
10
0
-10
****
YFP
α-PheRS
α-PheRS^Cys
N^RNAi
N^ICD
α-PheRS+N^ICD

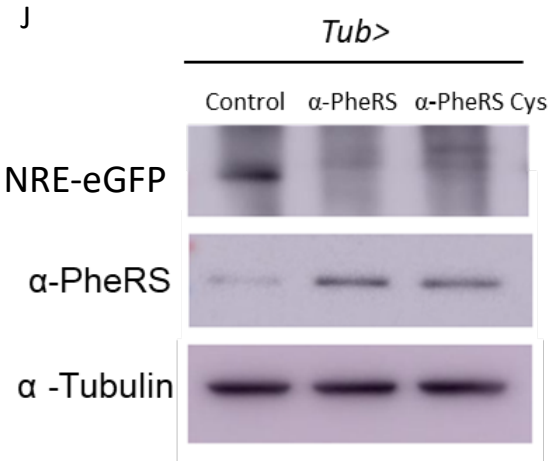
J
Tub>
Control
α-PheRS
α-PheRS Cys
NRE-eGFP
α-PheRS
α -Tubulin

Figure 3

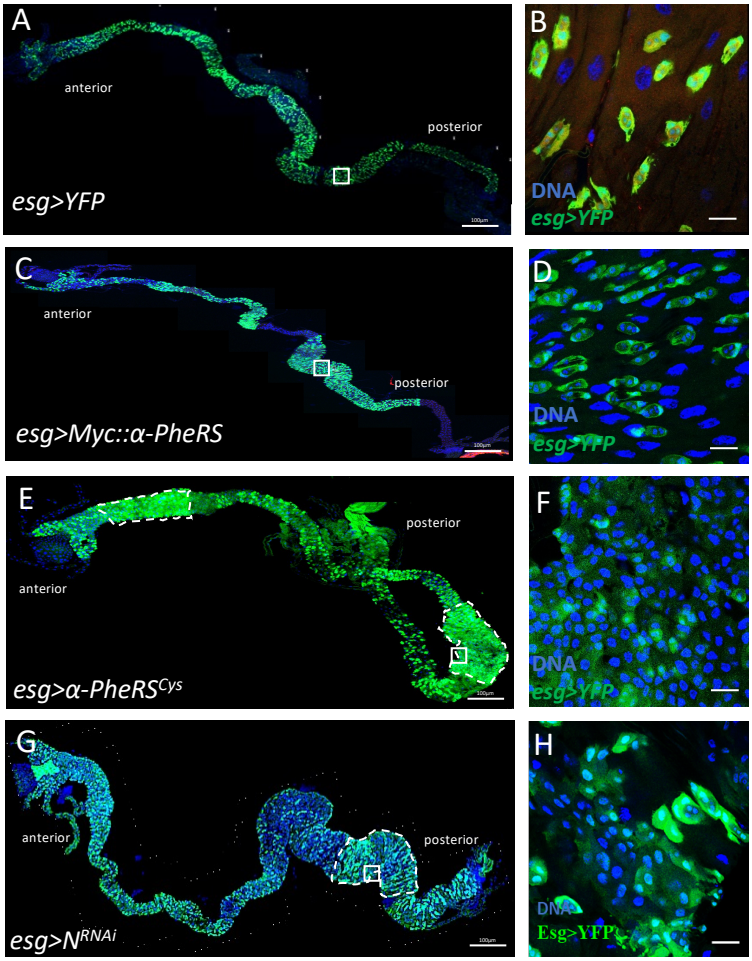
A
anterior
posterior
esg>YFP
B
DNA
esg>YFP
C
anterior
posterior
esg>Myc::α-PheRS
D
DNA
esg>YFP
E
posterior
anterior
esg>α-PheRS^Cys
F
DNA
esg>YFP
G
anterior
posterior
esg>N^RNAi
H
DNA
Esg>YFP

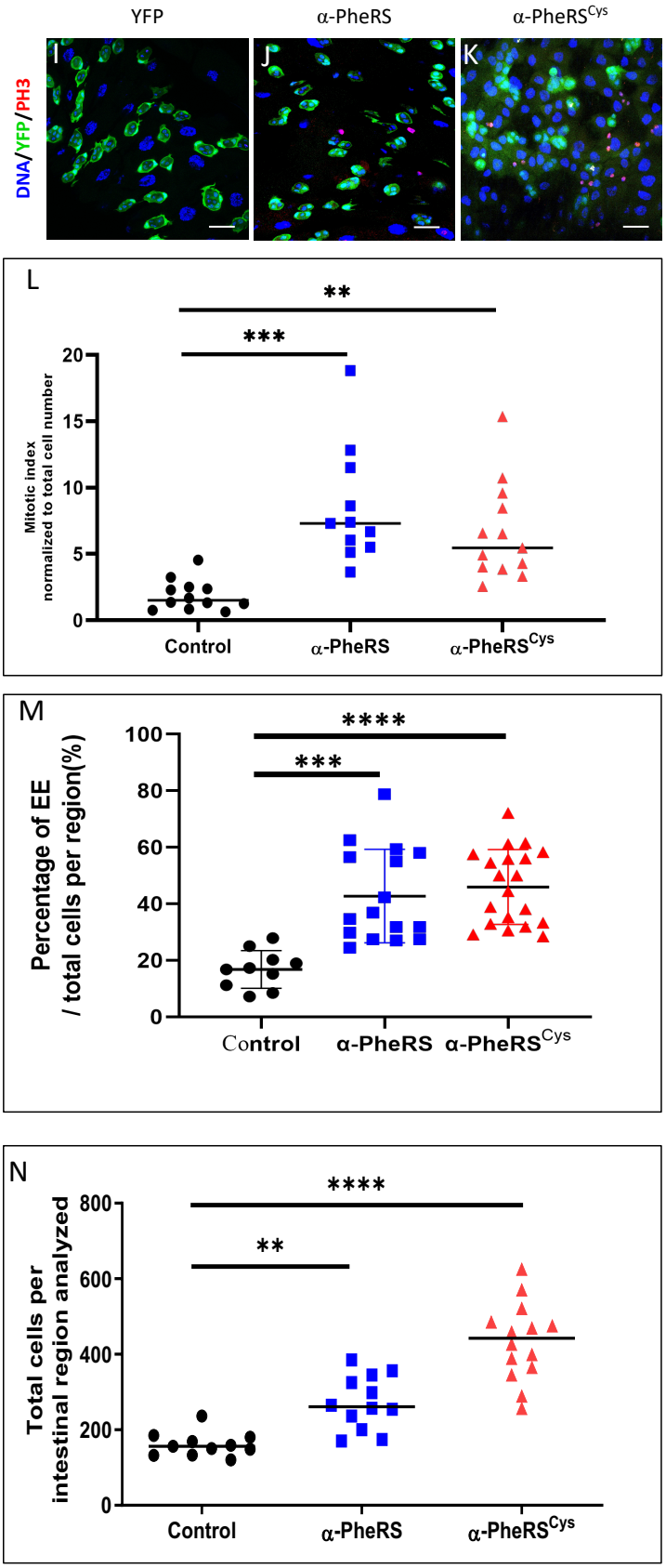
YFP
α-PheRS
α-PheRS^Cys
DNA/YFP/PH3
I
J
K
L
Mitotic index normalized to total cell number
Control
α-PheRS
α-PheRS^Cys
M
Percentage of EE / total cells per region(%)
Control
α-PheRS
α-PheRS^Cys
N
Total cells per intestinal region analyzed
Control
α-PheRS
α-PheRS^Cys

Figure 4

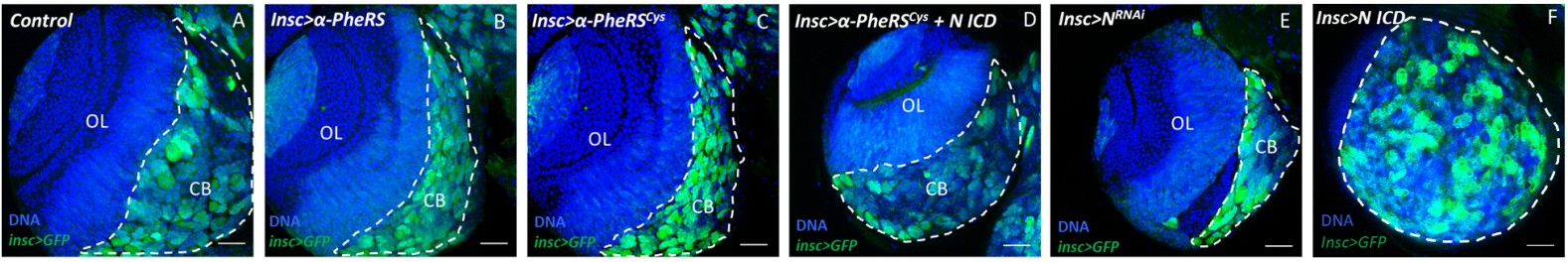
Control
A
OL
CB
DNA
insc>GFP
Insc>α-PheRS
B
Insc>α-PheRS^Cys
C
Insc>α-PheRS^Cys + N ICD
D
Insc>N^RNAi
E
Insc>N ICD
F

G

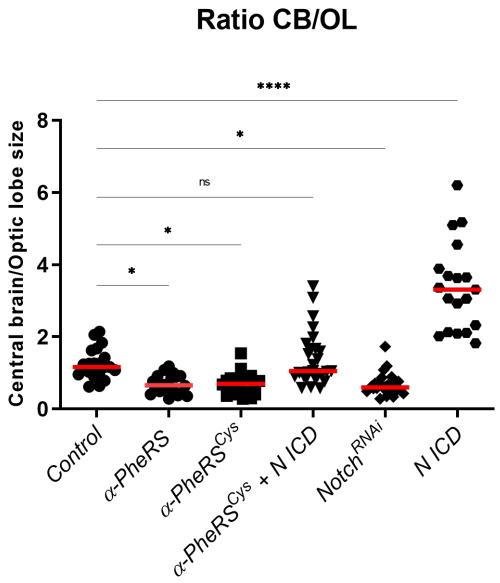
Ratio CB/OL
Central brain/Optic lobe size
0
2
4
6
8
****
*
ns
*
*
Control
α-PheRS
α-PheRS^Cys
α-PheRS^Cys + N ICD
Notch^RNAi
N ICD

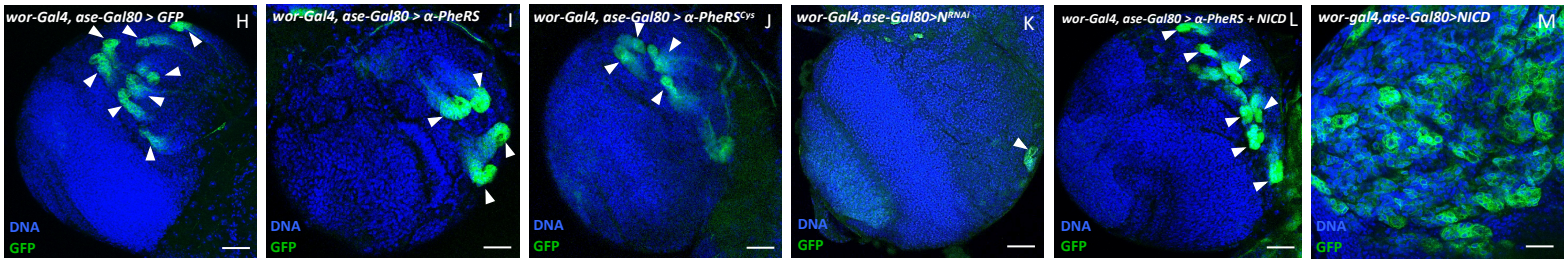
wor-Gal4, ase-Gal80 > GFP
H
wor-Gal4, ase-Gal80 > α-PheRS
I
wor-Gal4, ase-Gal80 > α-PheRS^Cys
J
wor-Gal4,ase-Gal80>N^RNAi
K
wor-Gal4, ase-Gal80 > α-PheRS + NICD
L
wor-gal4,ase-Gal80>NICD
M
DNA
GFP

N

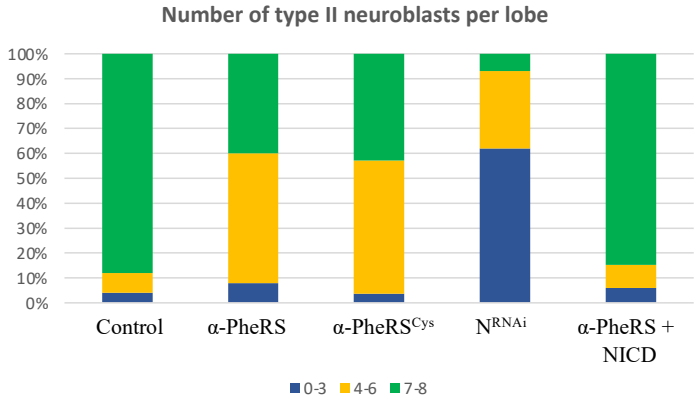
Number of type II neuroblasts per lobe
100%
90%
80%
70%
60%
50%
40%
30%
20%
10%
0%
Control
α-PheRS
α-PheRS^Cys
N^RNAi
α-PheRS + NICD
0-3
4-6
7-8

Figure 5

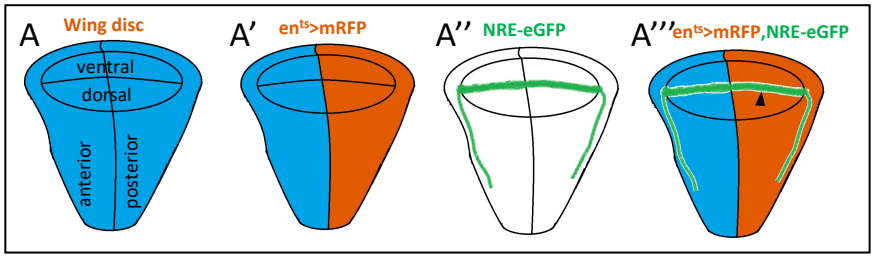
A
Wing disc
ventral
dorsal
anterior
posterior
A'
en^ts>mRFP
A''
NRE-eGFP
A'''
en^ts>mRFP,NRE-eGFP

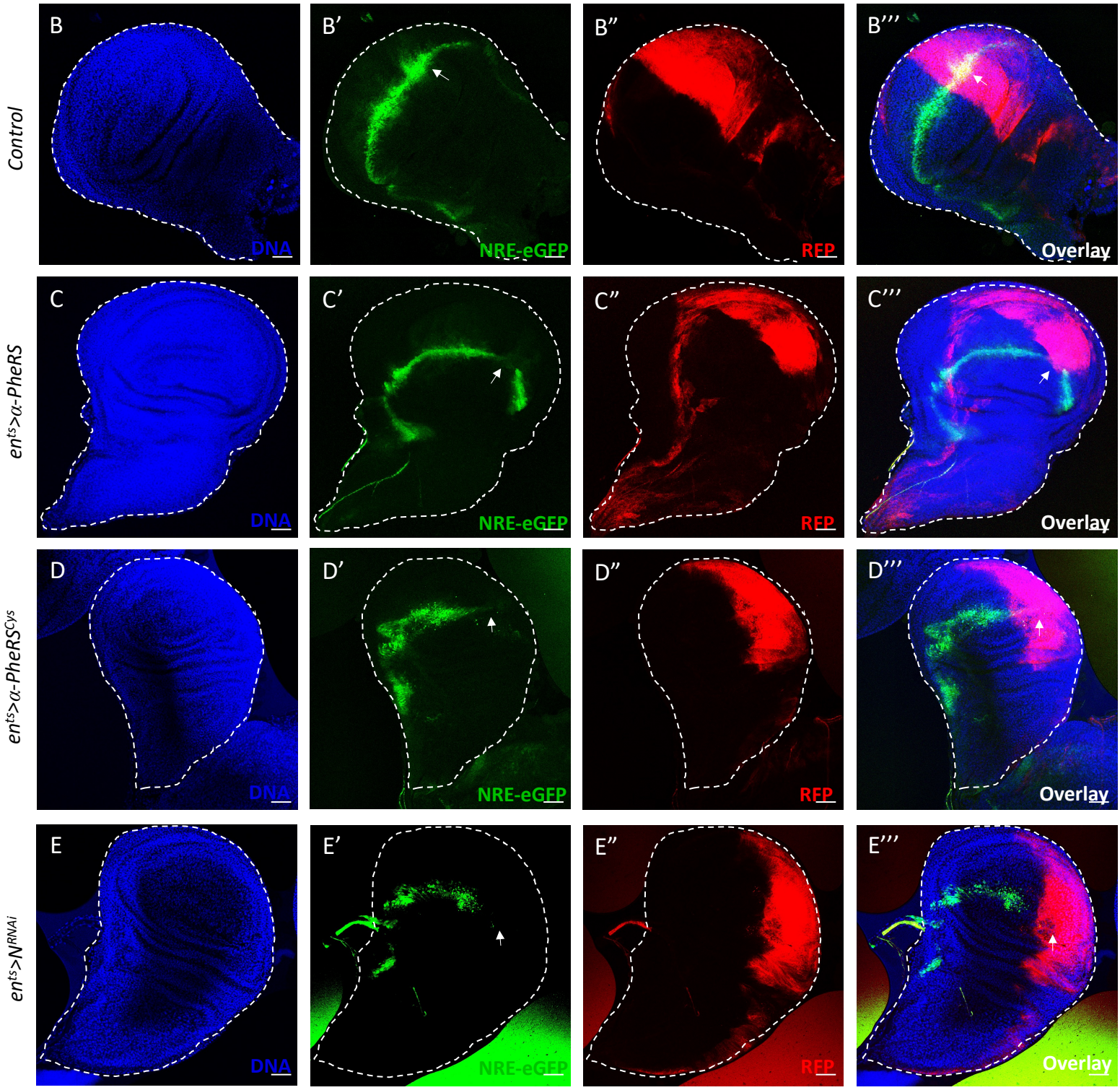
Control
en^ts>α-PheRS
en^ts>α-PheRS^Cys
en^ts>N^RNAi
B
B'
B''
B'''
C
C'
C''
C'''
D
D'
D''
D'''
E
E'
E''
E'''
DNA
NRE-eGFP
RFP
Overlay

Figure 6

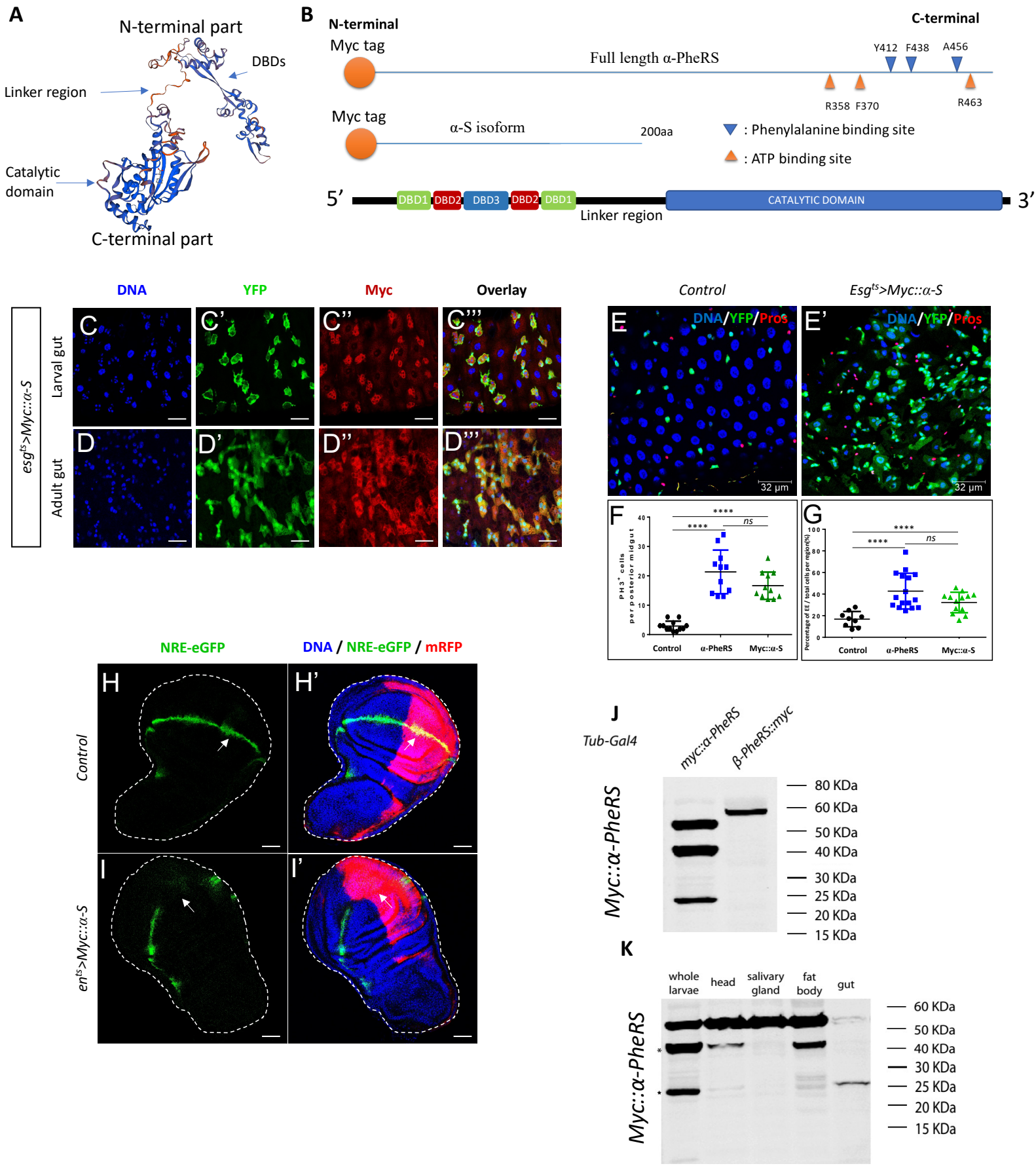
A
N-terminal part
DBDs
Linker region
Catalytic domain
C-terminal part
B
N-terminal
Myc tag
Full length α-PheRS
C-terminal
Y412 F438 A456
R358 F370
R463
Myc tag
α-S isoform
200aa
: Phenylalanine binding site
: ATP binding site
5'
DBD1 DBD2 DBD3 DBD2 DBD1
Linker region
CATALYTIC DOMAIN
3'
DNA
YFP
Myc
Overlay
esg^ts>Myc::α-S
Larval gut
Adult gut
C C' C'' C'''
D D' D'' D'''
Control
Esg^ts>Myc::α-S
E DNA/YFP/Pros
E' DNA/YFP/Pros
32 µm
F
PH3+ cells per posterior midgut
Control
α-PheRS
Myc::α-S
G
Percentage of EE / total cells per region(%)
Control
α-PheRS
Myc::α-S
NRE-eGFP
DNA / NRE-eGFP / mRFP
H H'
I I'
Control
en^ts>Myc::α-S
J
Tub-Gal4
myc::α-PheRS
β-PheRS::myc
Myc::α-PheRS
80 KDa
60 KDa
50 KDa
40 KDa
30 KDa
25 KDa
20 KDa
15 KDa
K
whole larvae
head
salivary gland
fat body
gut
Myc::α-PheRS
60 KDa
50 KDa
40 KDa
30 KDa
25 KDa
20 KDa
15 KDa

Figure 7

A

```
P07207 NOTCH_DROME   1681 GIQIYLEIDNRKCTECFTHAVEAAEFLAATAAKHQLRNDFQIHSVRGIKNPGDE--DNGE   1738
Q9W3J5 SYFA_DROME      25 --AALFAEDHQKIVGSLKSIQAHGELVTAE---------TVTHKSLGLTDEGRAVVENGS     73
                              :  *::* . .:.     .*:::*                *.  *:.: *    :**.
                                                                  RAM
P07207 NOTCH_DROME   1739 PPANVKYVI--TGIILVIIALAFFGMVLSTQRKRAHGVTWFPEGFRAPAAVMSRRRRDPH   1796
Q9W3J5 SYFA_DROME      74 HEALVYDLVPPEGIAQAA-LMAAGGANAKVGFSKAMSHGWILVDKSVTPP-LVRRKVDTI    131
                            * *  ::   **  .   :*  *   ..  .:* .  *.   .  .    : **: *
                                                                  RAM
P07207 NOTCH_DROME   1797 GQEMRNLNKQVAMQSQGVGQPGAHWSDDESDMPLPKRQRSDPVSGVGLGNNGGYASDHTM   1856
Q9W3J5 SYFA_DROME     132 TDVVRNQLQQVALGK-GDQLPAKEVAD----FKKRKLLQETTTKSFVLARGPEFATTLTK    186
                           : :**  :***: . *   *. . :*    :   *  :.  .... *...  :*:  *
                                                                  RAM
P07207 NOTCH_DROME   1857 ---VSEYEEADQRVWSQAHLDVVDVRAIMTPPAHQDGGKHDVDARGPCGLTPLMIAAVRG   1913
Q9W3J5 SYFA_DROME     187 LETDLTVEMLANGLWDQLKFKAYNFDALGAPPTRGH-------------LHPLLK-----    228
                                *   : :*.* ::.. :. *: :**:: .                * **:
```

RAM domain: 1766-1896; N-terminal of α-PheRS: 1-180

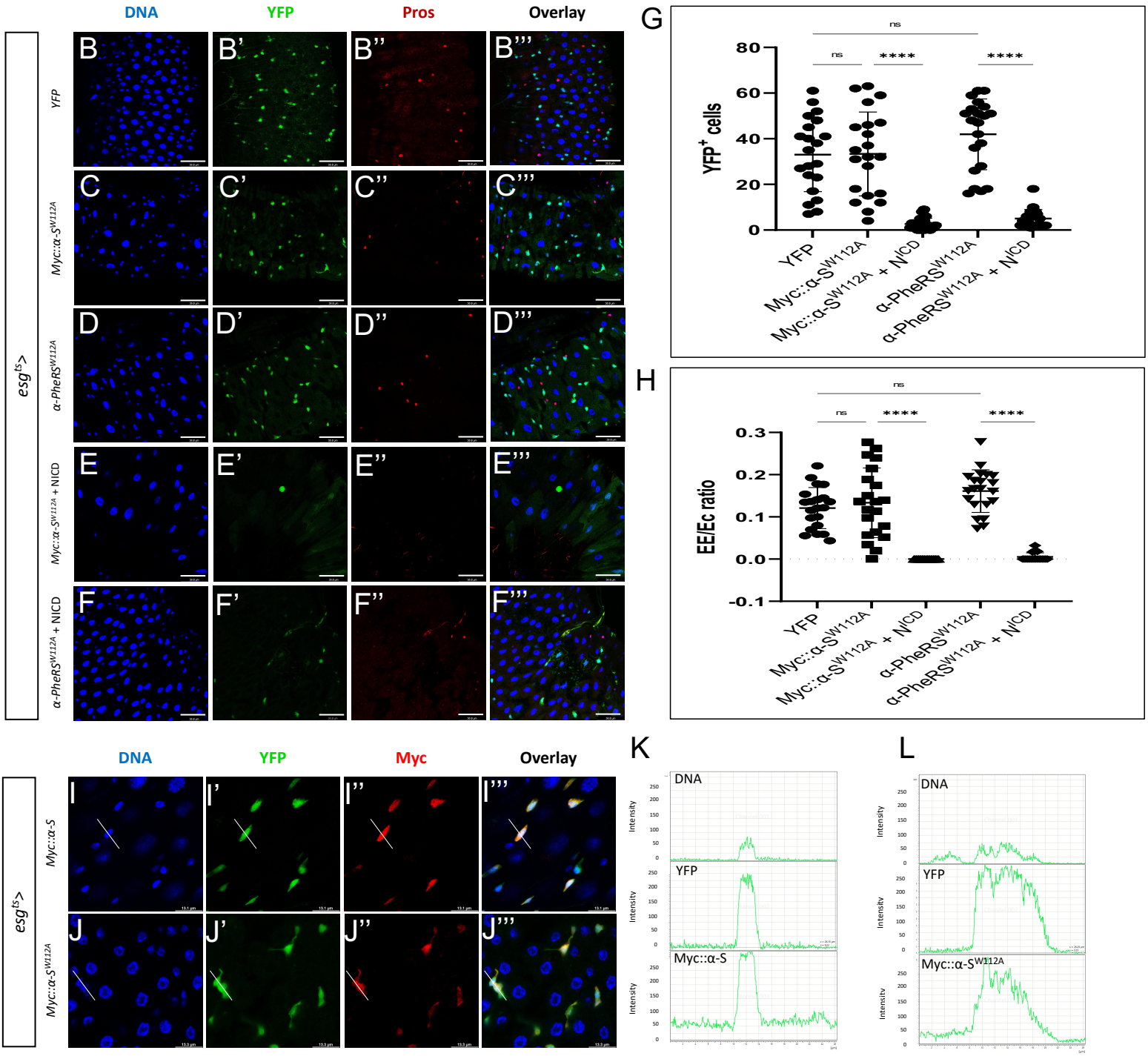

Figure S1

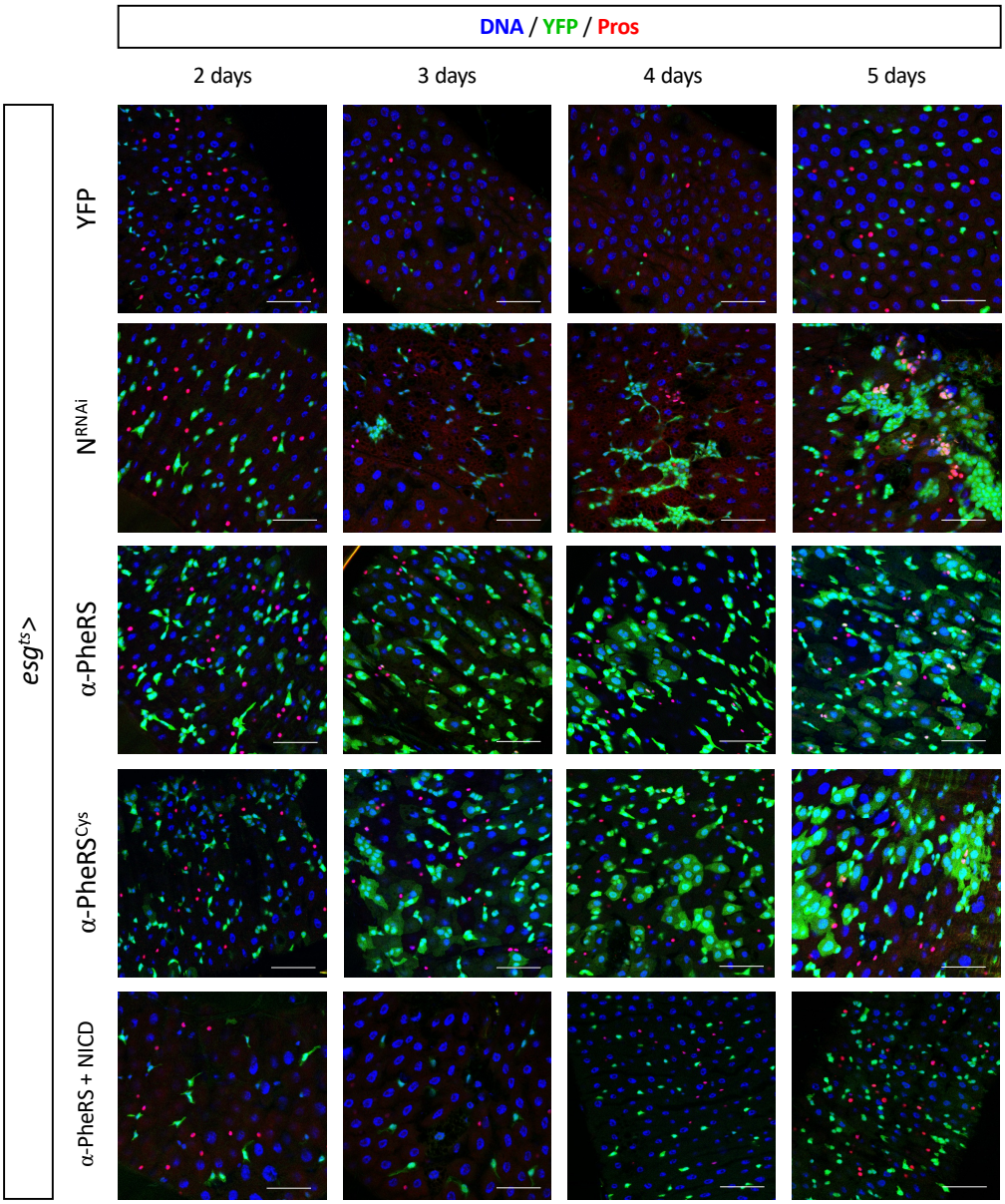

Figure S1: *α-PheRS* or *α-PheRS^{Cys}* were overexpressed using the *esg-Gal4,UAS-2XEYFP;tub-Gal80^{ts}* (=esg^{ts}) system that allowed us to control the expression time to study the kinetics of the appearance of the phenotypes. The kinetics of the *Notch* knockdown resembled partially the one of *PheRS$^{(Cys)}$* expression (esg^{ts} / *UAS-α-PheRS$^{(Cys)}$)*. Animals were mated at 18°C, and adults of the required genotypes were collected and shifted to 29°C to inactivate Gal80^{ts}. Adult midguts were dissected from female flies after the indicated induction times.

Figure S2

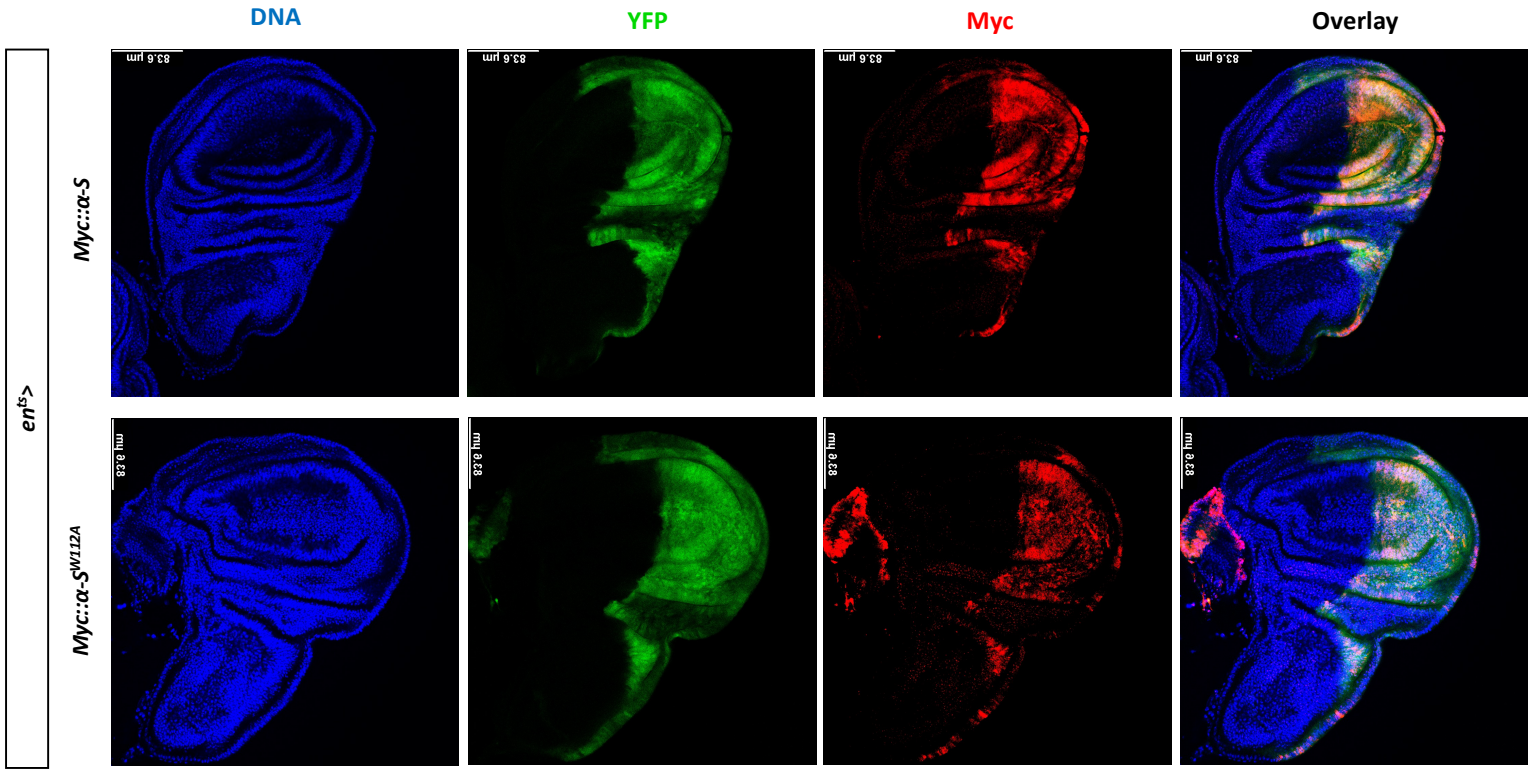

Figure S2: Staining wing discs for Myc::α-S showed the stable expression of both truncated alleles *Myc::α-S* and *Myc::α-S^{W112A}*. The *en-Gal4,UAS-EGFP;tub-Gal80^{ts}* (en^{ts}) system was used to drive transgene expression in the posterior compartment of developing wing discs (en^{ts}*/UAS-Myc::α-S* or *Myc::α-S^{W112A}*) and Hoechst staining to label nuclei. Animals were initially kept at 18°C for 3 days and then shifted to 29°C to inactivate Gal80^{ts} until adult flies hatched, enabling expression of Myc::α-S or Myc::α-S^{W112A}.

Figure S3

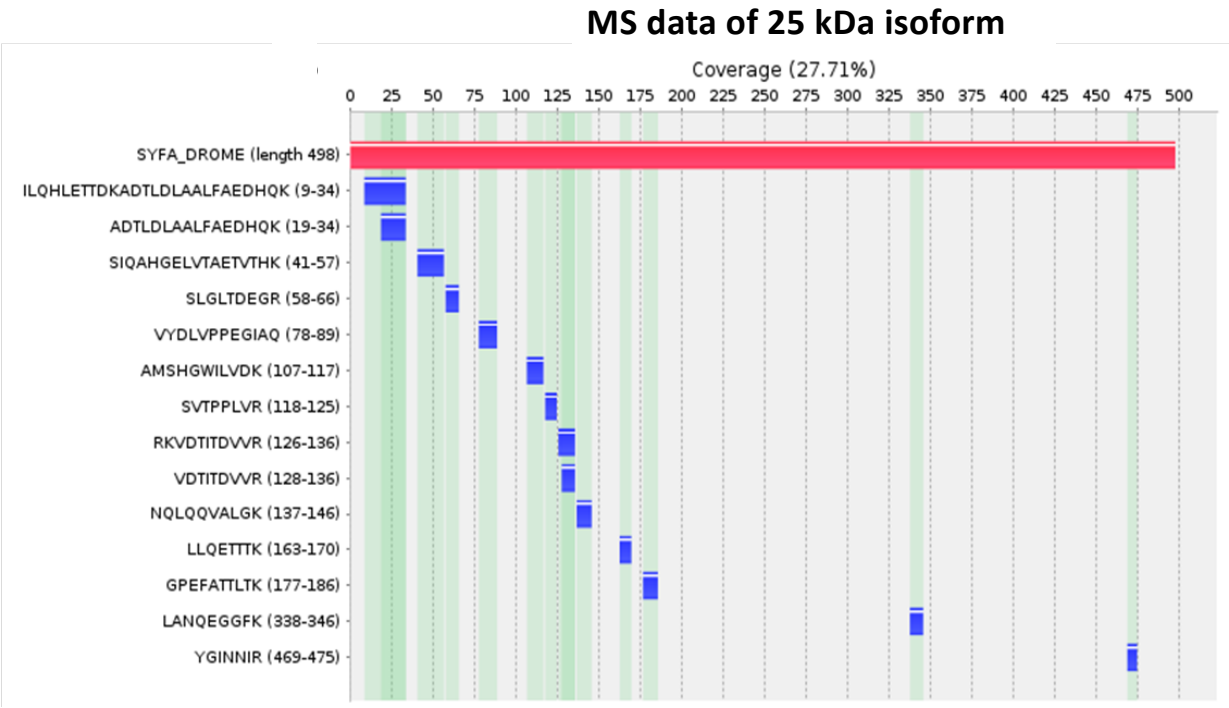

Figure S3: The Myc-tagged isoforms from whole larvae were purified by immunoprecipitation and gel purification. The tryptic peptide fragments of the 25kDa band were subsequently analyzed by mass spectrometry (MS). The MS data analysis revealed the peptide coverage of the 25KDa isoform according to the score of Peptide Spectrum Matches (PSM). The 25 KDa isoform contains the peptides of the N-terminal 28% of the full-length α-PheRS.

Figure S4

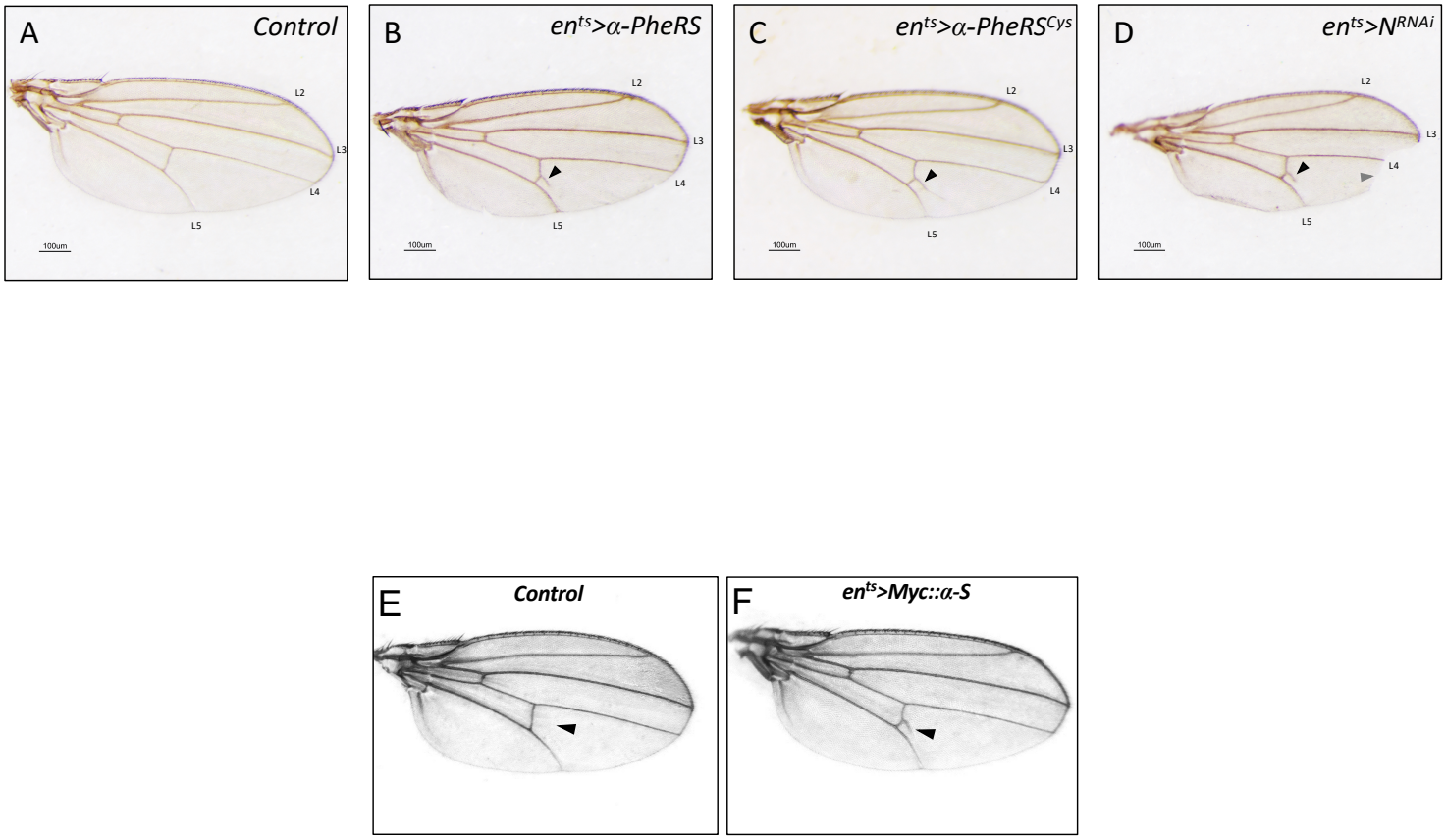

Figure S4: The ectopic wing venation phenotype resulting from elevated levels of α-PheRS$^{(Cys)}$ and α-S is similar to the phenotype of N^{RNAi} treatment. An ectopic vein branches from the connecting vein between the L4 and L5 vein (arrowhead in B-F). D) Knockdown of *Notch* shows this phenotype and the classical notched phenotype in the distal region of L3, L4, and near the L5 vein. The *en-Gal4,tub-Gal80^{ts}* (en^{ts}) system was used to drive transgene expression in the posterior compartment of developing wing discs *(*en^{ts}*/UAS-α-PheRS$^{(Cys)}$).* Animals were initially kept at 18°C for 3 days and then shifted to 29°C to inactivate Gal80^{ts} until adult flies hatched, enabling expression of α-PheRS, α-PheRS^{Cys}, α-S, or N^{RNAi}.